

**THESIS**

**RELATING SNOWFALL PATTERNS OVER THE CENTRAL AND EASTERN  
U.S. TO INFRARED IMAGERY OF EXTRATROPICAL CYCLONE COMMA  
HEADS**

Submitted by

Darren T. Van Cleave

Department of Atmospheric Science

In partial fulfillment of the requirements

For the Degree of Master of Science

Colorado State University

Fort Collins, Colorado

Summer 2009

COLORADO STATE UNIVERSITY

July 8, 2009

WE HEREBY RECOMMEND THAT THE THESIS PREPARED UNDER OUR SUPERVISION BY DARREN T. VAN CLEAVE ENTITLED RELATING SNOWFALL PATTERNS OVER THE CENTRAL AND EASTERN U.S. TO INFRARED IMAGERY OF EXTRATROPICAL CYCLONE COMMA HEADS BE ACCEPTED AS FULFILLING IN PART REQUIREMENTS FOR THE DEGREE OF MASTER OF SCIENCE.

Committee on Graduate Work

---

Dr. Susan C. van den Heever

---

Dr. Jeffrey D. Niemann

---

Advisor Dr. Thomas H. Vonder Haar

---

Department Head Dr. Richard H. Johnson

## ABSTRACT OF THESIS

### RELATING SNOWFALL PATTERNS OVER THE CENTRAL AND EASTERN US TO INFRARED SATELLITE IMAGERY OF EXTRATROPICAL CYCLONE COMMA HEADS

Geostationary satellite imagery is a valuable tool in the analysis and forecasting of a multitude of weather phenomena; in this study, it is applied to wintertime snowfall forecasting. It has been noted that the pattern of cloudiness seen in the comma heads of extratropical cyclones observed with Geostationary Operational Environmental Satellite 10.7  $\mu\text{m}$  imagery may be related to the swath of snowfall deposited by these cyclones as they affect eastern two-thirds of the United States. This study relates that imagery to snow swaths by categorizing extratropical cyclones. In an examination of 24 such cases spanning the last 13 years, three broad categories of cloud-top patterns emerged, each representing 8 of the 24 total cases. The first is the classic comma-head shape, for which there is a contiguous cloud shield covering both the comma head and the frontal zone; this is termed the classic category. In this category, the brightness temperatures within the cloud shield over the comma head are roughly the same as those over the frontal zones. The second category is characterized by a comma head which is distinct (in a brightness temperature sense) from the frontal cloud band; this is called the separated category. In these cases, the brightness temperatures over the cloud head indicate warmer cloud-top temperatures adjacent to the frontal zone. The third category is a separated comma head with cloud-top temperatures in the comma head warmer than in the frontal zone; this is referred to as the warm-separated category. It is observed that differences exist in the snowfall swaths occurring in the vicinity of the comma heads for the three categories.

North American Regional Reanalysis data is used to determine the differences in storm structures among the three categories which were responsible for the differing cloud patterns. In particular, composite maps and cross sections of various dynamic and thermodynamic fields are presented. It is found that a different jet position among the various cyclone categories creates varying ageostrophic circulations, with the weaker circulations being associated with separated comma heads. In addition, it is discovered that the presence of a trough (trough of warm air aloft) airstream in the classic cases is connected with the presence of a contiguous cloud shield, whereas its absence in the separated and warm separated cases is associated with the discontinuous comma head. It is shown that the classic cyclones produce a swath of snow co-located with the coldest cloud tops and spread throughout the southern half of the comma head, while the snow swath of the second and third categories is generally in a narrower band located to the southeast of the coldest clouds. Lastly, the warm-separated category is found to be associated a type of storm evolution which leads to strong cyclogenesis.

Darren T. Van Cleave  
Atmospheric Science Department  
Colorado State University  
Fort Collins, CO 80523  
Summer 2009

## ACKNOWLEDGEMENTS

First and foremost, I would like to thank my advisor, Dr. Tom Vonder Haar, for all of his advice and wisdom, not just pertaining to this thesis but in all facets of the graduate school experience. Without his direction and insight, none of this work would have been possible. Secondly, I would like to thank Jack Dostalek for his many helpful ideas and creative problem-solving ideas in developing this project. Both members of my committee deserve recognition, Dr. Sue van den Heever for her invaluable experience with atmospheric dynamics, and Dr. Jeffrey Niemann for his insightful comments about surface snowfall observations. I would also like to thank Chad Gravelle of Saint Louis University for providing me with snowfall maps for requested dates.

I would also like to recognize other people in the Colorado State University Atmospheric Science Department who have helped me in various theoretical and technical portions of this thesis. Dr. Wayne Schubert and Zach Finch provided help with coding the QG omega equation, Jeff Lemke created the conceptual diagrams, Dan Bikos, Jeff Braun, and Dr. Mark DeMaria all gave their insightful comments with regards to possible forecasting applications of this research, and Karll Renken and Hiro Gosden provided computing and software support.

Lastly, I would like to thank my room 301 office-mates, and all my family and friends for their support throughout this project.

This work was made possible through funding from the NOAA Grant NA17RJ1228.

## **TABLE OF CONTENTS**

**Abstract**

**Acknowledgments**

**Table of Contents**

**Chapter 1: Introduction**

**Chapter 2: Past Research**

2.1 Extratropical Cyclone Development and Classification

2.2 Extratropical Cyclone Dynamics

2.3 Use of Satellite Imagery to Forecast Heavy Snow

**Chapter 3: Datasets and Instrumentation**

3.1 GOES

3.2 COOP

3.3 NARR

**Chapter 4: Methodology**

4.1 Satellite Data

4.2 Case Collection

4.3 NARR Composite

4.4 Snow Swath Composite

4.5 Cross Sections

4.6 Omega

**Chapter 5: Results**

5.1 Thermodynamic Cause of Comma Head Separation

5.2 Comparison of the Present Cyclone Classification to Previous Studies

5.3 Snow Swaths

**Chapter 6: Conclusions and Future Work**

6.1 Causes of the Separated Comma Head

6.2 Forecasting Implications

6.3 Future Work

**References**

**Appendix 1: Forecaster Checklist**

**Appendix 2: Inconclusive Diagnostics**

## 1. INTRODUCTION

Despite recent advances in numerical weather prediction and in situ atmospheric observations, snowfall forecasting over the United States remains a difficult task. Weather forecast models often have flaws in the predicted track and intensity of cold-season extratropical cyclones, and important mesoscale features such as banded snowfall are poorly simulated because of limits in numerical weather forecasting. To compensate for these flaws, forecasters need to make use of other means of assessing the synoptic situation, such as conceptual models of extratropical cyclones, which can indicate possible areas of significant precipitation. It might be helpful for forecasters to first conceptualize broad synoptic-scale snowfall trends before moving on to individual forecasting techniques.

This study uses geostationary infrared satellite imagery to find broad trends in snowfall swaths as related to a classification of extratropical cyclones. This classification is based on a particular cloud-top temperature feature (a separated comma head) found in snowstorms over the central and eastern United States. Specifically, this research will attempt to explain the presence or absence of the separated comma heads, and then relate characteristics of snowfall swaths such as shape and position to the three cyclone categories.

This research began as an effort to relate snowfall patterns to infrared imagery from the GOES (Geostationary Operational Environmental Satellite) satellite. Initially, two

snowstorm cases were found wherein the snow swaths as seen in visible GOES imagery were very different. This difference seemed to be related to the infrared images of the cyclone comma heads, which were also very different. One snow swath featured dispersed local maxima while the other was broader and continuous. The infrared imagery showed different cloud-top temperatures as well as different structure for the two cases. It was thus decided to seek out other cases of well-defined snow swaths created by storms which featured an obvious comma head in infrared imagery. Nearly 50 such cases were found (see Section 4.2 for an explanation of the techniques utilized to find cases). It was quickly apparent that the cases could be divided into several categories based on the continuity of the cyclone's cloud shield. While most cases featured the prototypical example of a continuous cloud shield wrapping cyclonically around to the north of the surface low pressure center, several cases exemplified a discontinuity in the cloud shield. In these cases, the coldest cloud tops of the comma head were visibly separated from the frontal zone by an area of warmer cloud tops (the frontal zone mentioned here refers to the area extending roughly along the cold front southward from the northern tip of the cyclone). These cases did not completely fit the cyclone categorization schemes provided in earlier publications (Young, 1993, Evans et al., 1994, Semple, 2003). Additionally, it was discovered that the cases with "separated" comma heads featured a noticeably different snow swath than the "classic" comma-head cases. The separated comma-head cases had a more organized swath of heavier snow focused on the southern side of the comma head, whereas the snow swath of the classic cases tended to be more diffuse, spreading throughout the entire comma head with localized maxima.

The attempt to separate the cases into classic comma heads and separated comma heads based on cloud-top temperatures yielded yet another category: warm-separated comma heads. Some of the cases with discontinuous comma-head cloud shields featured comma heads with cloud-top temperatures that were notably warmer than their respective frontal zones. The snow swaths from these storms were similar to the standard separated comma-head cases in terms of shape and areal extent, although the measured snow totals were generally less. However, the differences in cloud-top structure and the probable thermodynamic differences were sufficient to merit the creation of a third cyclone category. Table 1.1 summarizes the differences of the three categories.

Table 1.1 – Summary of the characteristics of the three cyclone categorizations.

	Classic	Separated	Warm Separated
Comma-Head Clouds	Continuous throughout the cloud shield extending from the frontal zone to the tip of the comma head	Distinct separation between the comma head and the frontal zone, clouds in comma head are nearly as cold as those of the frontal zone	Separation between the comma head and the frontal zone, clouds in comma head are warmer than those of the frontal zone
Snow Swath	Broad with local maxima	Narrow structure extending ~ 100 km south of the coldest cloud tops	Narrow structure extending just south of the coldest cloud tops

The lack of detailed literature on separated comma heads, combined with the notable snowfall differences among the cyclone categories provided motivation for this research. Forecasting applications of this project were apparent: knowledge of connections between satellite imagery and resulting snow swath could be of use to forecasters.

## **2. PAST RESEARCH**

### **2.1 Extratropical Cyclone Development and Classification**

Since geostationary satellites first broadcasted cloud images, scientists have been trying to use that imagery to aid in understanding extratropical cyclone structure. Evans et al. (1994) examined satellite imagery of 50 cases of rapid maritime cyclogenesis in the 1970's and 80's to develop a cyclogenesis classification scheme for rapidly deepening cyclones (defined as a pressure drop of 10 mb or more in 6 hours). They observed four categories of cyclone development: emerging cloud head, comma cloud, left exit, and instant occlusion.

The emerging cloud head cases feature a cyclonically turning cloud bulge appearing to the north of a surface low within an existing baroclinic leaf. As time progresses, a dry slot appears on the southern side of the developing comma head and the bulge develops a comma shape. The cloud tops of the comma head cool rapidly to the point where they are virtually indistinguishable from the preexisting cloud band. Two meridionally-separated jet streams are present, one upstream of the surface low on the poleward side of the initial baroclinic leaf, and another downstream of the low and poleward of the northern cloud shield. The second category, comma cloud cyclones, consists of the organization of a cloud cluster several hundred kilometers upstream of a polar-front cloud band. In contrast to the previous category, the cyclogenesis occurs not within the baroclinic leaf, but instead within the upstream cloud cluster. As development continues, the jet along the baroclinic leaf weakens, and the jet upstream of the cloud cluster

strengthens and curves cyclonically along the poleward side of the newly-developed trailing cold front within the initial cloud cluster. The third cyclone category, the left exit, features the development of a baroclinic leaf poleward of and parallel to a preexisting baroclinic zone. As development continues, the baroclinic leaf appears to rotate cyclonically, and eventually merges with the baroclinic zone, wherein the cloud top temperatures of the two features become indistinguishable. A jet streak on the northern edge of the initial baroclinic zone becomes a cyclonically-turning jet within the cold front of the incipient cyclone, which is visually similar to the final stage of the first two categories. Lastly, the instant occlusion features a cold-air cloud cluster upstream of a polar frontal baroclinic leaf. The two features merge in a manner similar to the previous categories as cyclogenesis progresses, although differences exist. For example, the cold-air cloud cluster does not rotate and open cellular convection appears within the cloud cluster. The authors concluded that in the first three categories, the superposition of geostrophic shear and curvature vorticity advection occurring over the surface low enhances cyclogenesis. The instant occlusion category is slightly different, with confluent upper-tropospheric flow and lower-tropospheric static stability proposed to be the driving mechanisms behind the cyclogenesis.

Using the idea of principal airstreams or conveyor belts, Semple (2003) attempted a classification scheme based on previous publications cyclone categories, combining the various concepts into a single conceptual model. This was done by taking the most common elements of all the models, such as the concept of conveyor belts, and treating those elements as part of a continuum of storm evolution, rather than a discrete set of individual categories. This relaxation allowed for intermediate cyclones, that is, cyclones

could move from one category to another as they developed over time. Thus, less emphasis was placed on individual categories, and instead the focus was on the individual cyclone components such as conveyor belts.

Semple found that the warm-conveyor belt (WCB), defined as the airstream of high  $\theta_w$  (wet-bulb potential temperature) air rising from the southern to the northern ends of the cyclone in a system-relative framework, is one of the more important elements of storm structure, along with the cold conveyor belt and the jet position. The air within the primary warm conveyor belt originates in the lower troposphere on the southern side of the cyclone and turns slightly cyclonically on its northward path (Harrold 1973). The distinct western and poleward edges of the cyclone were found to be associated with interaction of the rising air of the WCB with sinking, dry, upper-tropospheric air from upstream of the cyclone. This configuration can be potentially unstable and can lead to elevated convection above the WCB, sometimes analyzed as an upper-level cold front. On its northern edge, the WCB typically curves anticyclonically in the downstream direction (recent research has shown that the WCB bifurcates and one of its branches forms the trough airstream as it turns cyclonically around the low, Grim et al. 2007). Similarly, the cold conveyor belt (CCB) originates in the colder air downstream of the cyclone, rising westward under the WCB, and finally either turning anticyclonically through the comma head or cyclonically around the low (Carlson 1980; Schultz 2001). These three airstreams (WCB, CCB, and dry airstream), along with the position of the jet, were used by Semple to describe the evolution of cyclones.

Semple defined the development of a cyclone as consisting of several stages of development. Initially, an enhanced convective cloud or a polar-front cloud band forms

along a jet streak. If the jet streak cuts into the polar-front cloud band, a convex-poleward bulge is witnessed in a feature commonly called a baroclinic leaf. In the next stage of development, a comma head develops in one of two ways: either a continuous jet throughout the system creates a distinctly warmer comma head in comparison to the clouds associated with the WCB, or a jet consisting of two parts, one on the poleward side of the system and one upstream of the cold front, create a visibly continuous comma head. As the cyclone continues to develop, the westward isentropic rise of the CCB results in the westward extension of the comma head. The CCB bifurcates west of the surface low into two parts: one ceases ascending and rotates cyclonically around the surface low, and the other continues to ascend as it rotates anticyclonically to the north of the cyclone (Schultz 2001). The comma head thus transitions from a product of the WCB to the CCB. Further development causes a frontal fracture between the surface warm and cold fronts; a stage which involves the intrusion of mid-level dry air and requires the presence of two jets as in the second category of comma-head development. If the cyclone develops further, the air of the dry intrusion overruns the second WCB and eventually the vorticity of the systems becomes vertically stacked from the surface to the upper levels.

Semple summarized this work by demonstrating how the cyclone categorization schemes of the past fit into the developmental stages previously summarized. It was shown that the various cyclone classification schemes merely represent perturbations of basic cyclone elements such as the WCB, the CCB, and the jet streaks. The evolution of these features could describe the life cycle of an extratropical cyclone, Semple theorized. In concluding the paper, he matched these results with past publications by demonstrating

pictorially how various perturbations of the life cycle stages could fit past conceptual models.

Young (1993) created a manual for weather forecasters on diagnosing cyclogenesis from satellite imagery. He identified four types of cyclogenesis as part of a flowchart to assist in forecaster decision-making: meridional trough, split flow, cold-air vortex or instant occlusion, and flat trough.

The meridional trough cyclogenesis is characterized initially by a broad upper-trough and associated baroclinic leaf. Similar to Semple (2003), Young notes that the baroclinic leaf is really a large WCB, with air originating at low levels on the southern side ascending as it moves northward. As the storm progresses, potential-vorticity advection results in a secondary warm conveyor belt extending rearward from under the baroclinic leaf and characterized by strong ascent. Meanwhile, a middle and upper-level dry slot is entrained in the system to the south of the secondary WCB. The second cyclogenesis category, split flow cyclogenesis, begins with two meridionally-separated jets (similar to the emerging cloud head case of Evans, 1994), an anticyclonically curved cirrus shield within a deformation zone downstream of an upper-trough, and an upstream short wave. When the shortwave catches up with the cirrus shield, the clouds of the shortwave take on a comma shape and merge with the preexisting cirrus region (although the two cloud features are visually distinct), and the southern jet curves cyclonically around the inside of the new trailing cold front. Finally, the two cloud features merge completely into a large comma cloud as the northern jet is positioned along the northern cloud boundary and the southern jet turns cyclonically around the surface low pressure.

Young's third cyclogenesis category consists of two types: cold air vortex and instant occlusion. The instant occlusion category is similar to Evans (1994) and features a baroclinic leaf upstream of a trough and an upstream baroclinic cloud feature driven by a jet streak at its rear. As the upstream feature nears the baroclinic leaf it becomes comma-shaped, and the rearward jet streak merges with the jet on the northern side of the baroclinic leaf. The two cloud systems eventually merge, and the associated comma head becomes pronounced as it wrapped around the surface low. The closely-related cold-air vortex classification differs in that the upstream cloud feature possess no baroclinicity and dissipate as it approaches the baroclinic leaf, with the baroclinic leaf itself bulging on the northern side into a comma head. The final category is flat-trough cyclogenesis, wherein the driving upper-level trough is "flat" in the sense that the curvature of the geopotential heights is limited at its base. This category features a comma head which protrudes out from under the baroclinic leaf as it develops.

## **2.2 Extratropical Cyclone Dynamics**

There are many ways to investigate the dynamics and associated precipitation of extratropical cyclones. Individual authors often have their own preferences of which type of dynamics to look at. Some prefer analyzing jets and jet locations (Uccellini et al., 1987), some focus on the dry air intrusion or trowal (Martin, 1999), others like to look at instability considerations (Moore et al., 2005), while other authors have their own preferred diagnostics (Dixon et al., 2002). To accommodate the needs of this present study, this section will focus on previous work that used jet locations and trowal dynamics to explain cyclone dynamics, because these parameters best address the results of this study.

Uccellini and Kocin (1987) explored the relationship between jet streak circulations and snowfall over the eastern United States. The authors looked at eight major snow events from the winters of 1983 to 1987. The 300 mb winds for the cases were treated as the jets, with the data being derived from radiosonde observations analyzed onto a grid. All of the cases were found to feature some type of double-jet configuration; that is, two meridionally-separated jets, one on the northern border of the system and extending upstream, and another jet which was usually turning cyclonically around the south and east of the surface low. The authors noted that the jet positions for all of the cases were such that the ageostrophic circulations of the two jets reinforced each other. The northern jet caused a thermally direct “transverse” (perpendicular to the jet direction) ageostrophic circulation along its entrance region. This circulation led to rising motion in the right entrance region of the jet, consistent with the convergent and divergent regions of an idealized jet (Beebe et al., 1955). Meanwhile, the southern jet featured a thermally indirect transverse ageostrophic circulation, causing rising motion in the left exit of the jet. Cross sections of the storms oriented roughly latitudinally revealed that the jets were indeed reinforcing each other. The two circulations were readily apparent in the cross sections, and when omega (atmospheric vertical motion) was plotted on top, it was shown that the reinforcing circulations were causing a broad area of slantwise rising motion between the two jets. It was also noted that the indirect circulation of the southern jet created a low-level jet at the surface which was capable of transporting moisture northward, one of the necessary ingredients for snow. The authors concluded that the jet circulations were of definitive importance for forecasting heavy snow.

Hakim and Uccellini (1992) looked at ageostrophic jet-streak circulations in a northern plains snowstorm. This time, in place of the relatively coarse and unreliable radiosonde network, the researchers used an operational weather forecasting model, the NGM (Nested Grid Model), to create jet cross sections. As in the previous paper, cross sections of the transverse ageostrophic circulation were created; once again, they clearly depicted a thermally indirect circulation around the exit region of a southerly jet, a thermally direct circulation around the entrance of a northerly jet, and a broad area of slantwise rising motion in-between. However, whereas the radiosonde data of the previous study only allowed for cross sections to be computed every 12 hours, the operational forecast model provided cross sections every six hours, providing more frequent diagnosis of the storm. Because of the increased temporal resolution, the authors were able to track the two circulations individually as the jets approached each other. It was discovered that the near-merger of the two jets (when the circulations coupled) caused a period of more intense rising motion between the two, hypothesized to be caused by latent heat release. The authors pointed to modeling studies wherein latent heat release within jet streaks was found to strengthen and narrow the updraft. In similar fashion to the previous paper, the researchers concluded that the jet coupling was definitively responsible for at least a part of the observed slant-wise rising motion between the two jets and the resulting snowfall.

Some authors prefer to look at mature extratropical cyclones in terms of occlusion and trowal development in the northeast cyclone sector. Martin, for example, has authored several papers on the subject. Two papers of interest to this study are his 1998

publication on the occlusion process and 1999 article on QG (quasigeostrophic, an idealized atmospheric state) forcing in the vicinity of the trowal.

Martin (1998) looked at a single storm in January of 1995 over the central United States. The paper was released in two parts. For the first part, using the UW-NMS (University of Wisconsin Nonhydrostatic Modeling System) model running at 40 km grid spacing, the author performed a numerical simulation of the cyclone in order to understand the occlusion processes which took place. By tracking the 309 K  $\theta_e$  (equivalent potential temperature) surface which was representative of the warm and cold frontal intersection, it was found that cyclonic turning northeast of the surface low wrapped the 309 K  $\theta_e$  surface over itself in the vertical sense, which was a three-dimensional manifestation of the trowal. Using isentropic analysis, Martin calculated air parcel trajectories from various source regions of the cyclone airstreams, and was able to verify the “classic” occlusion process (a cold front “catching up” with and overriding a warm front) by noting that a representative air parcel from with the original cold front indeed traveled up and over the warm front. The author further noted that while this did seem to confirm the classical occlusion model, the overriding occurred first at middle and upper-tropospheric levels, rather than at the surface. Martin concluded the first part of the publication by hypothesizing that a certain potential-vorticity signature could be considered as an indication of the classic occlusion process taking place. In the second part of the publication, Martin again analyzed the same 1995 storm. For this section, he looked at symmetric instability associated with the “wrap-around” precipitation (another term for the area of the comma head) and air parcels tracking through the trowal. Martin

concluded that ascent of warm, moist air within the trowal portion of the storm was at least partially responsible for the heavy snowfall band.

Martin (1999) looked at QG forcing within the occluded sector and trowal airstreams of three extratropical cyclones. As in the previous publication, the UW-NMS model was used to simulate the thermodynamic variables of the storms, this time with 80 km grid spacing at 6 hour intervals. To visualize the processes taking place in the trowal airstreams of the storms, three-dimensional plots of isotropic  $\theta_e$  surfaces were generated, as well as air parcel tracks. One significant finding from this analysis was that the QG forcing of vertical motion within the occluded sector of cyclones was primarily a result of synoptic-scale processes, not frontal processes. This agrees with one of the findings of Martin's 1998b paper, that occlusion occurs first at mid-levels, not at the surface, indicating the "classic" model of occlusion as a frontal process is incorrect. Also in accordance with his previous papers, Martin concluded this paper by attributing the clouds and precipitation north and west of the occluded surface low to a "trowal airstream" which was thermodynamically separate from the classic WCB and CCB (similar to the secondary WCB of Young, 1993, later verified by Grim et al., 2007). This trowal airstream originated in the warm sector, turned cyclonically, and rose rapidly along the trowal. Martin linked the western extension of the observed comma head with the trowal air stream instead of an anticyclonically rising CCB as found in other publications.

Recent research has verified the existence of a secondary WCB in the form of a trowal airstream and has continued to emphasize its importance in clouds and precipitation within wintertime extratropical cyclones (Moore et al., 2005, Han et al., 2007, Grim et

al., 2007). Moore et al. (2005) investigated a storm which produced heavy snow within a long and narrow swath (>6 in. for ~1000 km), yet featured a relatively weak surface cyclone with a minimum surface pressure of only 1008 mb. Moore found that the trowal airstream contributed both to the depth and amount of moisture available to the northwest of the surface low, and stated that it was the most likely cause of the deeper clouds of the comma head. Grim et al. (2007) used data from a field campaign to investigate two winter storms over the Great Lakes region, and discovered that the snow swaths of both storms were co-located with the trowal airmass. They found that the trowal resided above the warm front, and was bordered to the south by a dry air intrusion which they termed as an upper-level humidity front. Han et al. (2007) performed model simulations on the same two cases and found that a circulation which was set up around the trowal lead to rising air within the trowal and sinking air in the dry airmass to the south. They attributed the snow swaths of both storms as well as their patterns in satellite and radar imagery to the aforementioned circulation in the vicinity of the trowal.

### **2.3 Use of Satellite Imagery to Forecast Heavy Snow**

As mentioned elsewhere in this study, geostationary satellite imagery is invaluable to forecasters in that it provides near real-time information about the atmosphere on a continuous basis for the entire forecasting area. Several authors have attempted to use geostationary satellite imagery in snowfall forecasting, because it provides information on location and development of pertinent storm dynamics. Two such publications are discussed in this section.

Beckman (1987) gathered 34 cases of snowstorms through the early to mid 1980's over the central United States with snowfall of at least 4 inches covering at least a portion

of two states with the intention of relating the observed snowfall pattern to satellite imagery. Analyses of the various cases yielded four apparent categories of central U.S. snowstorms: high plains cyclogenesis, southwest flow shortwave trough, northwest flow shortwave trough, and orographic. High plains cyclogenesis referred to storms that developed in the lee of the Rocky Mountains, usually around the state of Colorado. They were the longest-lasting of the four categories with durations of 12 to 18 hours, and were usually the largest with a width of around 300 km and a length between 600 and 1300 km. The majority of the events were of the southwest flow shortwave trough variety, which occurred over a wide area from Kansas to the Great Lakes to the Ohio Valley and lasted six to twelve hours. A few cases were classified as northwest flow shortwave troughs, which occurred over the Great Lakes area, were fairly short-lived, and propagated in a direction similar to convective-season severe weather outbreaks in that area. The last category, orographic storms, referred to cyclogenesis in the lee of the Rockies over New Mexico, which was the main type of snowstorm affecting the southern areas of the region of study.

Using the aforementioned cases, Beckman put together an analysis methodology for forecasters involving several types of observations; the third step of this methodology involved the use of satellite imagery. Beckman recommended first using satellite imagery to classify the storm according to the four snowstorm categories mentioned earlier, which provides the forecaster with a rough estimate of storm longevity and snowfall potential. From that point, Beckman provided several things to look for in satellite imagery. First, he suggested noting changes in infrared cloud top temperature and size as these attributes are associated with rising motion and storm development.

Next, Beckman suggested looking at the shape of cloud edges in the infrared imagery and texture in the visible, which, depending on whether they are rough or sharp, can indicate moisture availability. Lastly, Beckman recommended using the imagery to look for convective clouds within the storm, as they are usually associated with the heaviest snowfall.

Johnston (1995) reviewed several papers on the topic of using infrared satellite imagery in snowfall forecasting, and also introduced his own technique. In summarizing earlier papers, he noted that for strong winter storms, satellite imagery is mostly useful as a support tool during the event, because conventional forecasting models usually have a good handle on the storm dynamics. In weaker storms wherein forecasting models do not perform as well, certain precursor features in the satellite imagery can be useful in predicting snowfall. Johnston suggested that for these weaker storms, it is beneficial to consider an area termed the “shear zone”, which is a narrow region usually southeast of the comma head across which there is an abrupt change in the horizontal wind component. The author found that the heaviest snow in many of these “weaker” cases was located just to the left (upstream) of the shear zone, which happened to be on the southern tip of the comma head, as noted in Beckman (1987).

This present study will seek to expound upon this previous research by blending concepts from these previous studies. This research will blend the jet stream position work of Uccellini and Kocin (1987) with the trowal work of Martin (1998), while at the same time using satellite data, reanalysis data, and surface observations to investigate these features.

### **3. DATASETS AND INSTRUMENTATION**

#### **3.1 GOES**

Since its inception in 1975, the GOES (Geostationary Environmental Satellite) program, a part of NOAA (National Atmospheric and Oceanic Administration), has provided invaluable information about the atmosphere from a geostationary perspective. The GOES system is comprised of two geostationary satellites over the equator, one at 135° West and one at 75° West, usually referred to as GOES-West and GOES-East respectively (Menzel and Purdom, 1994). The location of the satellites allows them to scan not only the continental United States and North America, but also the entire hemisphere of the Earth facing the satellite, known as a full disk scan. The GOES instrument payload changes over time as new satellites are launched, but is generally comprised of visible and infrared imagers, as well as an infrared sounder.

GOES satellites are given a letter name while in production and a number after successful launch and placement into orbit, wherein they are expected to last at least five years. All launches have been successful with the exception of GOES G; thus, as of this writing, GOES A through N have been launched and GOES 1 through 13 have been operational. These satellites can be grouped in three series, where each satellite within a series has roughly identical construction and instrument payload. GOES A through H represent the first generation of GOES satellites, and were launched between 1975 and 1987. Several key problems hampered the first GOES series: imaging and sounding could not be performed at the same time, and the sounder only viewed Earth 5% of the

time, which precluded high temporal resolution data (Menzel and Purdom, 1994). Thus, NOAA began work in 1985 to create a new series of satellites addressing these issues as well as others, and in 1994, GOES I was launched. This series of satellites continued from GOES I through M; all of the imagery for this study was obtained by satellites within this series.

As mentioned previously, the primary GOES instrumentation is an imager and a sounder. For GOES I through M, the imager consists of a five-band spectrometer. The bands are (a) 0.52-0.72  $\mu\text{m}$  (visible), (b) 3.78-4.03  $\mu\text{m}$  (shortwave infrared window), (c) 10.2-11.2  $\mu\text{m}$  (longwave infrared window), and (d) 11.5-12.5  $\mu\text{m}$  (infrared window with more sensitivity to water vapor). The visible band features 1 km pixels (in the nadir direction) in the visible channel and 4 km pixels for the infrared and water vapor channels, while onboard calibration provides brightness temperatures with 1 K absolute accuracy and 0.3 K relative precision (Menzel and Purdom, 1994).

This study diagnoses cloud systems associated with extratropical cyclones over the central and eastern United States at all hours of the day, and thus GOES-East infrared imagery is used (see Section 4.1 for a more detailed explanation). Over the span of cases collected, 1996 to 2008, two satellites served as GOES-East: GOES 8 from 1996-2003 and GOES 12 from 2003 to 2008. This means that about half of the cases of extratropical cyclones used in this study featured infrared imagery from GOES 8, and the other half from GOES 12; because they are both from the I-M series, these satellites have nearly identical configuration and instrumentation.

### 3.2 COOP

The National Weather Service Cooperative Observer Program (COOP) has provided climate data for the United States since 1890 through a network of observers ranging from unpaid volunteers to employees of the National Weather Service. While most observing stations are homes or farms, some are associated with military bases, colleges and universities, state climate centers, federal agencies, and National Weather Service offices (NCDC, 2006). The number of currently active stations is about 8,000. Data from COOP locations is stored and stewarded by the National Climatic Data Center (NCDC), which is a part of the National Oceanic and Atmospheric Administration (NOAA).

One dataset produced by the COOP network and distributed by NCDC is the Surface Daily Land Summary of the Day, referred to as DSI-3200. This dataset contains records of precipitation, maximum and minimum temperature, and snowfall for 24-hour periods reported at a consistent time, usually 0700 local time. That is, each entry contains the previous day's meteorological measurements. Considerable effort has been exerted by NCDC to ensure a standard time of observation; however, because of the individual scheduling needs of the volunteer observers, standardized observation times are all but impossible. The DSI-3200 dataset thus includes date and time of observation, maximum-minimum temperature readings, snowfall, and total liquid-equivalent precipitation. Although 24-hour precipitation is the primary intent of the COOP program, a minority of stations also include wind measurements, observed weather, evaporation, and soil moisture.

The NCDC has taken steps to ensure data integrity through a system of manual and computerized quality control. The data are evaluated against surrounding stations, compared to climatological limits, subjected to internal consistency checks, and accessed serially. A system of quality control flags is used to mark data based on the quality control results. Occasionally, edits are made to the data when needed; these edits are flagged accordingly in the data file. By far, the data collected by principal observing stations (paid observers usually associated with federal agencies or universities) are considered the most accurate. These data are available under a separate dataset, DSI-3210, but is also included in DSI-3200.

For this present study, the DSI-3200 dataset was selected because it contains the largest number of stations giving the best available spatial resolution of observations. This presents two primary complications: accuracy of observations and time of observations. Fig. 3.1 shows a plot of time of observations for a representative case. The standard observation time of 0700 hours is apparent as the two most frequent observation times in the plot (the observations are obtained at 0700 local time, thus the two most frequent observation times represent the two most common time zones of the dataset); however, there are also a number of observations scattered about on either side of the peak. This casts some uncertainty as to the exact time of snowfall. An observer might take a measurement when snowfall ended instead of the mandatory observation time. Another observer may take two measurements for the same storm. These discrepancies preclude the use of daily plots of snowfall for that storm because the two datum points have different types of time-dependent information. Thus, for this study, snow swaths (the entire spatial coverage of snowfall created by a storm) rather than daily totals were

analyzed. In terms of accuracy, it was assumed that standardized and calibrated gauges, adequate training in observation procedures, and NCDC quality control result in a sufficiently accurate dataset.

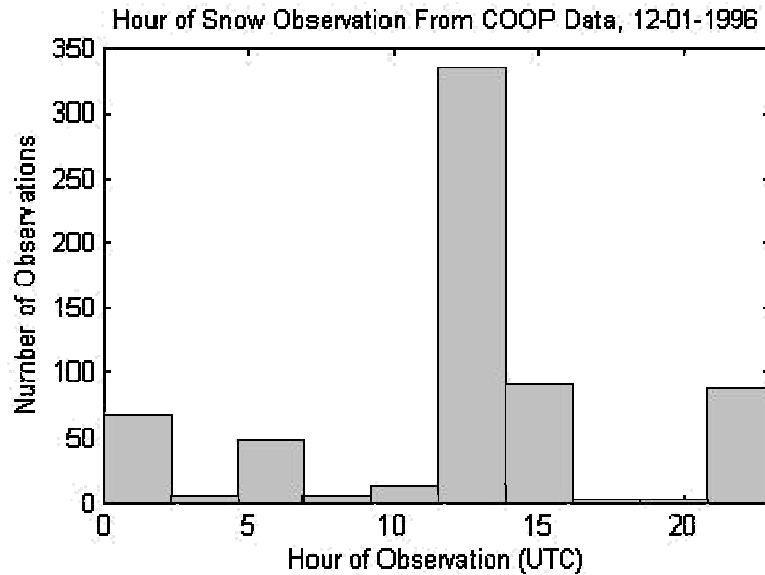


Fig. 3.1 – Histogram of hour of observation for COOP daily snow reports, 1 Dec. 1996.

### 3.3 NARR

Gridded fields of thermodynamic variables were obtained from the NARR (North American Regional Reanalysis) dataset (Mesinger et al., 2006). The NARR dataset was selected because of its temporal and spatial resolutions as well as its period of record. The NARR data are available every three hours dating back to 1979, and the output is exported on a lambert conformal conic projection with 32 kilometer horizontal resolution and 47 vertical layers averaging 50 millibar vertical resolution (Rutledge et al., 2005).

The NARR model is fundamentally a reanalysis operation using the NCEP Eta model (Mesinger et al., 2006) and the associated 3D variational data assimilation system (3DVAR). The Eta version within the NARR model is the operational version used in 2003, with the model physics and cloud parameterizations “frozen” at that time. That is,

in order to ensure internal consistency between different computational runs that contribute to the NARR dataset, no subsequent changes to the Eta model have been incorporated into the NARR. The model was developed as a successor to the GR2 (Global Reanalysis) model, with the primary purpose being realistic simulation of surface hydrological processes; however, testing of the model revealed that it also performed well with upper-air fields such as winds and temperatures, demonstrating the model to also be a good source of reanalysis for tropospheric dynamics. Specifically, Mesinger et al. (2006) found that root mean square fits of NARR data to rawinsonde data showed that the NARR data was usually within 4 m/s of the rawinsonde measurements. This level of accuracy demonstrates the desirability of the NARR data for this present study, given the importance of upper-level winds within this study.

## 4. METHODOLOGY

### 4.1 Satellite Data

The GOES-East data for this study were obtained from CIRA (Cooperative Institute for Research in the Atmosphere) archives. These archives contained dependable data dating back to 1996, and thus cases of extratropical cyclones were sought for the winters of 1996/1997 up to 2008. For most of the cases of interest, data were available at the typical CONUS (Continental United States) scan times of 15-minute intervals. Infrared imagery, specifically longwave GOES channel 4, was selected because of its 24-hour availability (the cases in this study occurred at all hours of the day, thus necessitating the 24-hour coverage). The archived satellite data was segmented into an eastern CONUS projection for displaying in McIDAS (Man computer Interactive Data Access System), a satellite imagery software package.

As is common with infrared satellite imagery, an enhancement table was applied to augment the colder cloud tops. Raw infrared imagery contains counts ranging from 0 to 255 representing infrared radiance; calibration and enhancement tables are used to convert counts to brightness temperatures and colors respectively. For this study, the CIRA standard infrared enhancement table was used, as well as the standard GOES IR calibration. For the calibration, satellite counts from 0 to 175 are converted linearly to temperatures with a count of 0 representing 330 K and a count of 175 representing 242.5 K (Clark, 1983). Counts higher than 175 are also converted linearly, but at a steeper slope than the lower counts, with a count of 255 representing 163 K. For the

enhancement table, a grayscale is used for temperatures from 330 K to 242.5 K, with colder temperatures using a color-map interpolating in order from yellow, red, magenta, green, and blue (yellow represents warmest brightness temperatures, blue represents coldest). The purpose of this is to provide more contrast for the colder cloud-tops as they tend to be the areas of greater interest. Table 4.1, 4.2, and 4.3 show this enhancement table applied to GOES 10.7  $\mu\text{m}$  imagery. This enhancement table happens to be the default for AWIPS (Advanced Weather Interactive Processing System), which is used by NWS (National Weather Service) forecasters nationwide. Therefore, cloud features of interest to this study (most notably the separated comma head, see Section 6.1) which are most apparent because of the enhancement table used will also be seen by NWS weather forecasters, assuming they use the default enhancement table.

## **4.2 Case Collection**

A comprehensive search was performed for cases of extratropical cyclones over the central and eastern United States. Other parts of the country were excluded for several reasons: (a) cyclones over the intermountain west tend to lose structure due to orographic interferences, (b) cyclones immediately in the lee of the Rockies undergo lee cyclogenesis, meaning that storms in this vicinity are rapidly evolving and may not have a consistent structure, (c) cyclones over the East Coast often fall into the category of Nor'easters, a special case of storm development (Zishka and Smith, 1980). Furthermore, COOP snowfall observations were only available over the United States, effectively excluding from consideration any oceans as well as Canada. Therefore, the area of interest for this study was from about 75° to 100° West, and from 33° to 49° North. These restrictions lead to most of the analyzed storms being of the high plains

cyclogenesis or southwest flow shortwave trough variety as categorized by Beckman (1987).

Cyclones were sought that featured a “textbook” comma head, meaning a broad cloud shield wrapping cyclonically around the north of a surface low, as well as snowfall measurements of at least five inches (an amount arbitrarily chosen to eliminate smaller storms from consideration). The snow swaths of interest located via the COOP plots were checked against composite satellite, radar, and surface observations available from NCAR (National Corporation for Atmospheric Research) to verify their applicability for this study. If a particular cyclone met both of the two aforementioned stipulations, satellite imagery was then obtained for the time period of interest.

The case search yielded about 50 cases of extratropical cyclones with snowfall observations of at least five inches for the period 1996 to 2008. The cases were placed into the three categories mentioned in Section 1 based on the cloud fields: classic comma heads, separated comma heads, and warm separated comma heads. Eight of each type were discovered, narrowing the total number of cases to 24; the other 26 cases did not completely fit any of the three cyclone categories, and were thus eliminated from consideration.

Classic cases were defined as having a frontal-zone length of at least 1000 km as seen in infrared satellite imagery, and a comma head extending upstream of the frontal zone at least 500 km (Fig. 4.1). Cases wherein the comma head wrapped cyclonically around the low to the point where the comma head was south of the low center were excluded, because the initial purpose of the study was to investigate precipitation to the northwest of the low. Cloud-top temperatures from the frontal zone through the comma head varied

by no more than 15 K, meaning that the comma head appeared continuous in the satellite imagery. Separated cases were defined as having an area of cloud tops within the comma shield on the order of 30 K warmer than the surrounding frontal zone and comma head, thus making a visible separation between the two. This area of separation was at least 200 km wide, while the remaining comma head was at least 450 km long by 250 km wide with cloud-top temperatures within 15 K of the average temperatures of the frontal zone. The last category, warm separated, had no spatial requirements because the comma head tended to be smaller and more diffuse than the separated comma-head cases. The primary definition for the warm separated cases was comma-head temperatures averaging at least 15 K warmer than frontal-zone temperatures. In contrast with the separated comma-head cases, the warm-separated cases did not exhibit the same distance of separation in the infrared imagery. Rather, the distance of separation (while still evident) was as little as 50 kilometers, and the cloud tops within the area of separation were about 20 K warmer than the colder regions of the comma head. The warm separated cases were named as such because, as mentioned earlier, the coldest regions of the comma head were still at least 15 K warmer than the frontal zone.

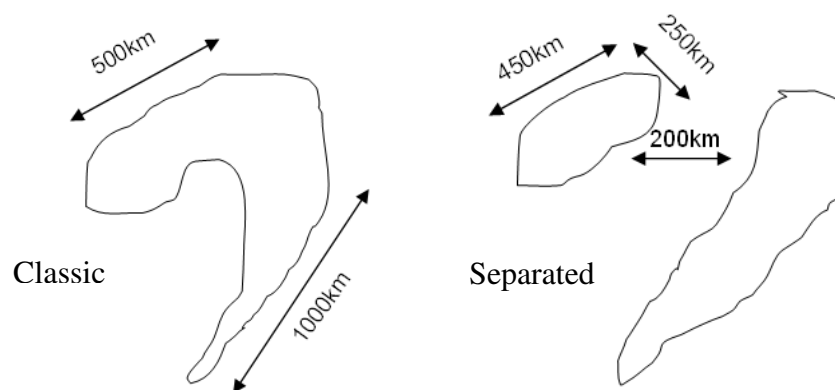


Fig. 4.1 – Schematics of the cloud shapes for two cyclone categories as seen in infrared imagery.

These definitions create distinct extratropical cyclone classifications, similar to Evans et al. (1994). This is in contrast to Semple (2003), wherein a spectrum of cyclone development was used in place of discrete categorization. The use of discrete categorization within this study was justified because the satellite imagery for the entirety of the storm lifetimes revealed that there were virtually no transitions of a given cyclone from one category to another. While the separated comma heads of the warm-separated cases often reconnected with their respective frontal zones (see Section 6.2.), the resulting cyclone structure was never fully equivalent to that of the classic cases. Specifically, the storms at this point of development often obtained the structure of a Nor'easter, a cyclone type which was purposely excluded from the classic categorization as mentioned earlier. The classic cases, meanwhile, never featured a separated comma head throughout their lifetimes over the U.S. (storms were not analyzed once they moved offshore as discussed in Section 4.3).

#### **4.3 NARR Composite**

The storm-relative composites utilized in this study required a remapping of the NARR data from its native lambert conformal conic projection to a uniform latitude-longitude grid. The native NARR projection features grid boxes which are uniform in horizontal size but not oriented normally to latitudinal lines. For this study, plotting and compositing required the grid boxes to be equally-spaced in a latitude-longitude sense, and oriented normal to lines of latitude. Thus, before processing and analysis of NARR data took place, the 32 km x 32 km NARR data was first remapped within MATLAB onto a  $0.25^\circ \times 0.25^\circ$  equirectangular projection grid using triangle-based linear

interpolation. After interpolation, noise was reduced by applying a rotationally symmetric Gaussian lowpass filter to all grid points surrounding a point of interest.

Three model times for each case were utilized in making the composites. The first hour was selected as the hour in which the storm first met the criteria for the desired cyclone category. For the classic cases, this was the hour in which the comma head first began to extend cyclonically around the low, or the hour in which the trailing frontal zone first formed a continuous cloud shield extending the requisite 1000 km to the south of the low. For the separated and warm separated cases, the first hour was the time at which the comma head separated from the main frontal zone or cooled to temperatures within the requisite threshold derived from the category definition. The last hour for the classic cases was defined as either the hour the storm evolved to a structure which no longer met the spatial requirements of the classic cyclone definition, or more commonly the hour wherein the storm moved outside of the area of data coverage (this did not adversely affect the study because storms which continued to strengthen as they moved outside the area of data coverage were usually deep, occluded vortexes with dimensions uncharacteristic of the classic category by the time they moved outside the area). The last hour for the separated and warm separated cases was the time at which the comma head began to warm and dissipate, or the time at which the distance of separation between the comma head and frontal zone began to decrease below the chosen threshold. For all cyclone categories, the middle hour was then defined as the hour between the first and last hours. Because the NARR data are only available every three hours, this methodology required the first and last hours to be selected in such a way as to allow a center hour at a midpoint between the two. For the separated and warm-separated cases,

the total life-span wherein the cyclone met the category definitions was usually 6-12 hours. The classic cases were longer-lived with typical life-spans of 12-18 hours. Tables 4.1 through 4.3 show all the cases at the various composite hours for each of the three categories.

Table 4.1 – Infrared imagery of the compositing hours for each of the classic cases.

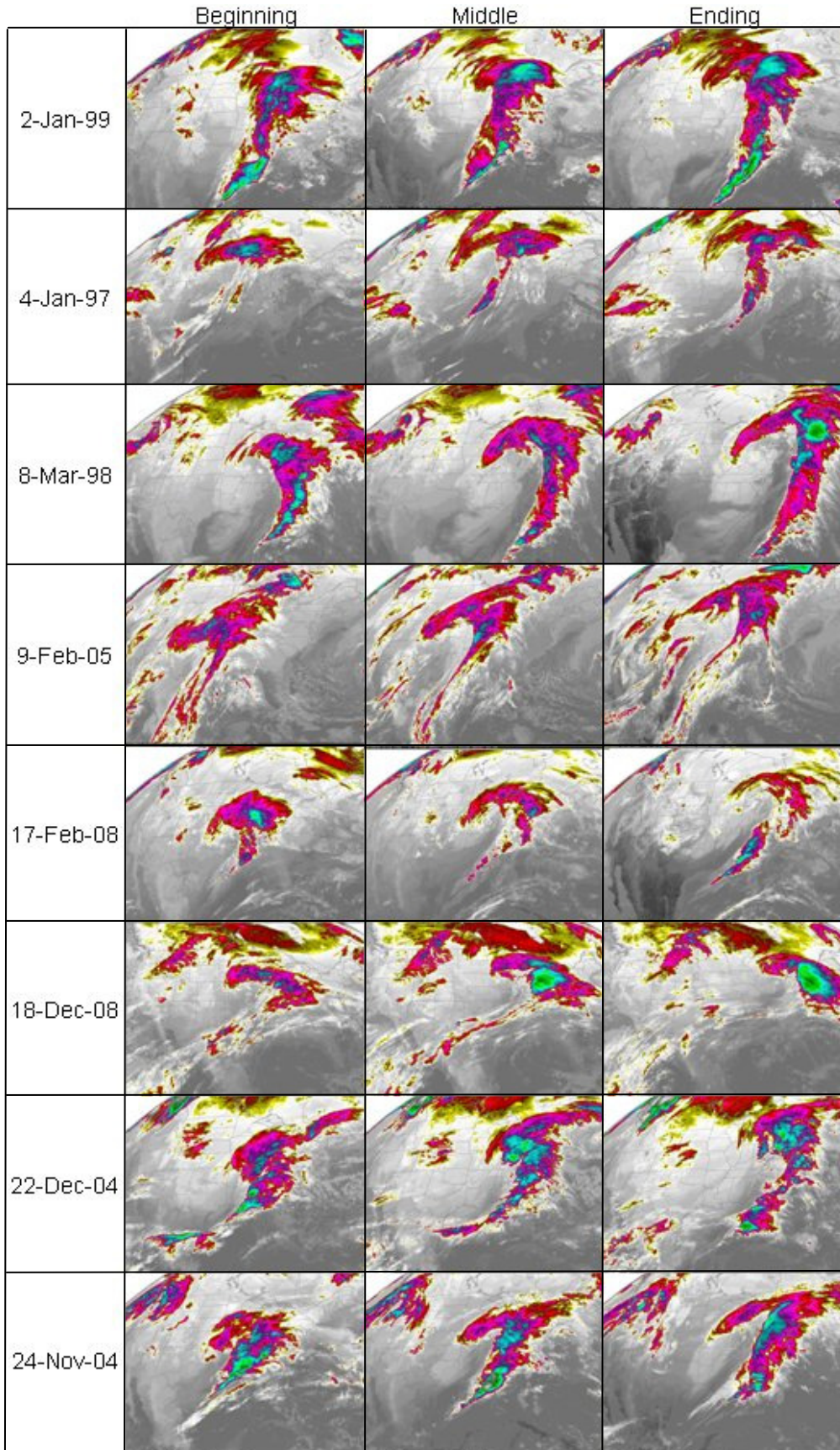


Table 4.2 – As in Table 4.1, except for the separated cases.

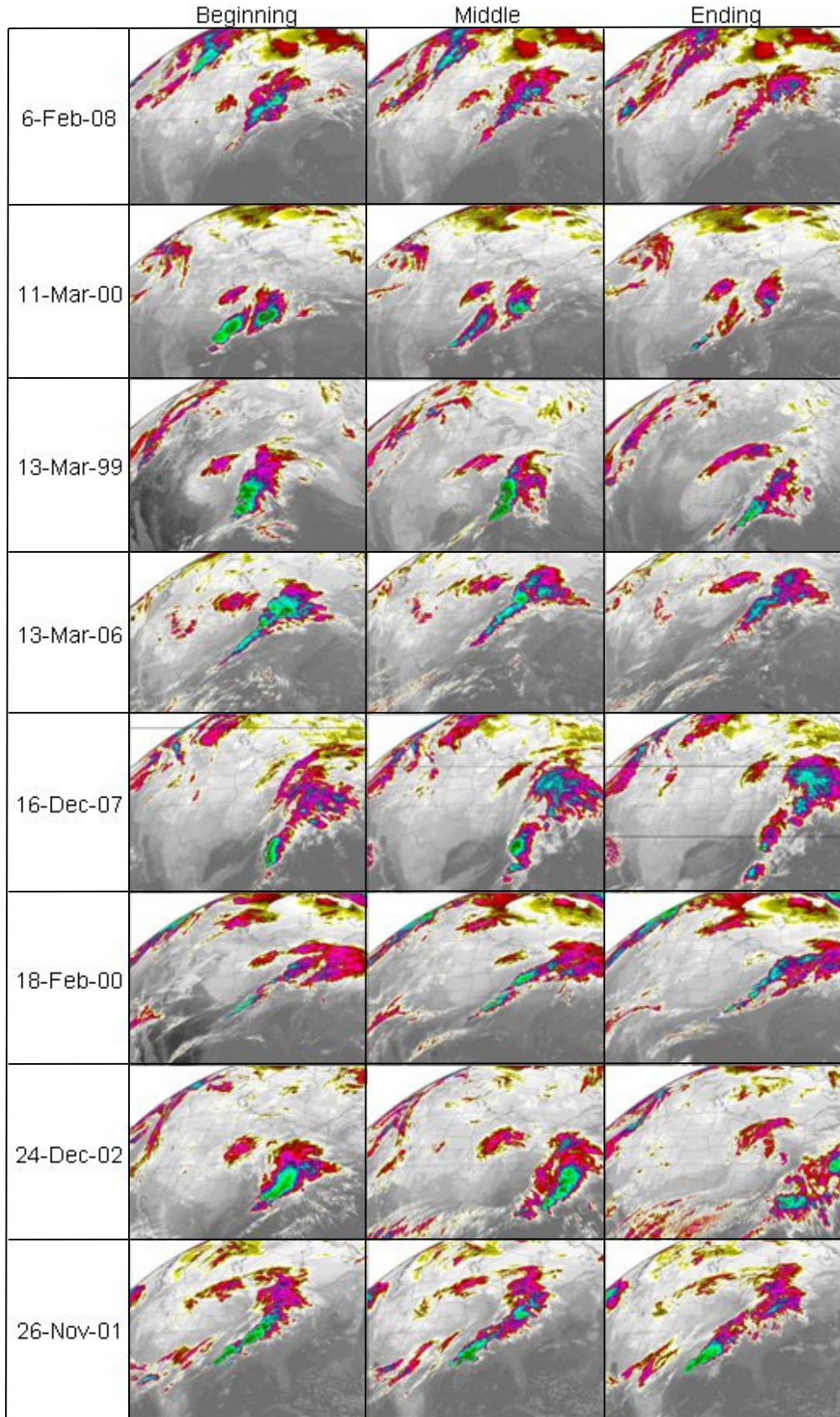
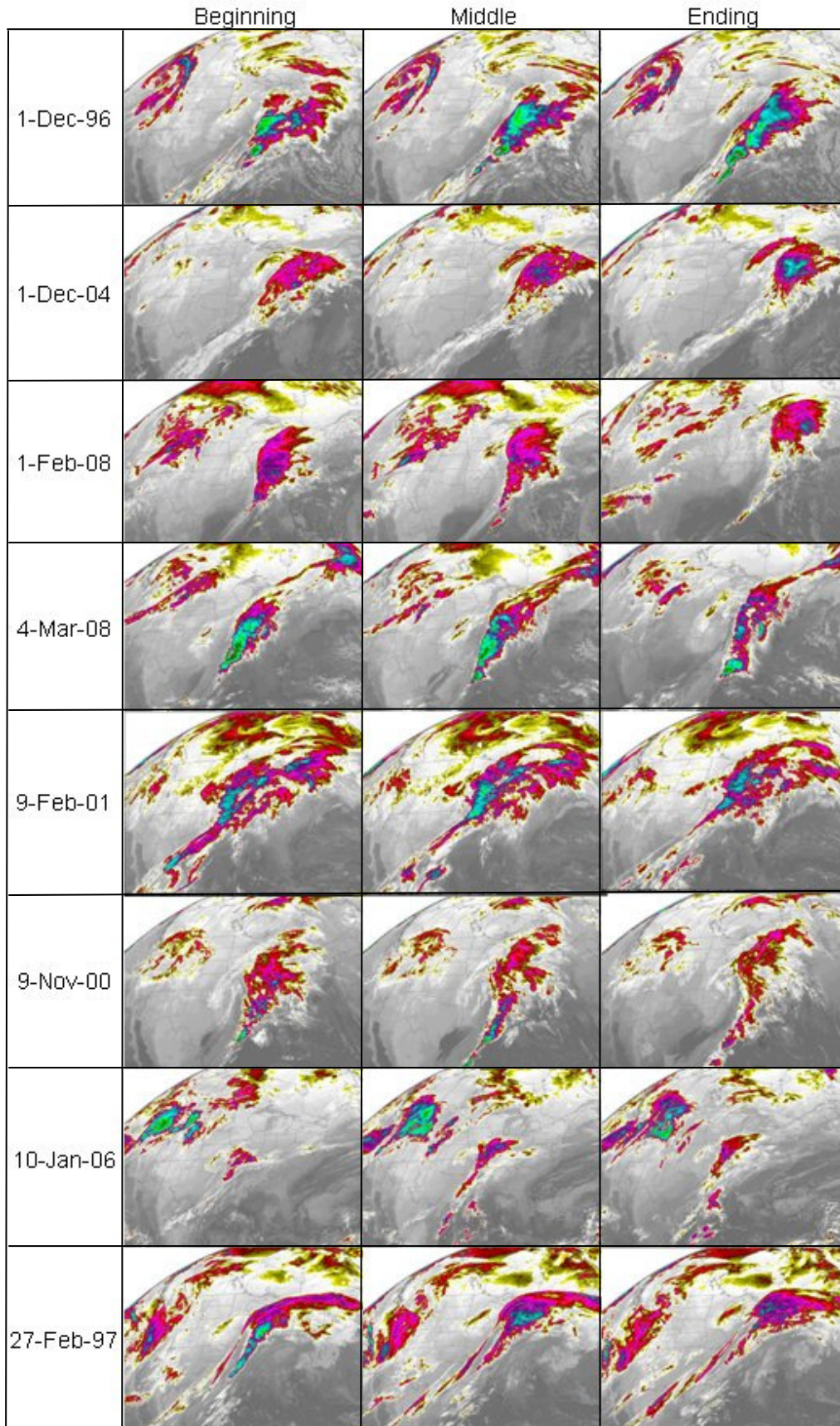


Table 4.3 – As in Table 4.1, for the warm-separated cases.



After the compositing hours were determined for all cyclone categories, the composites were calculated at the desired compositing hour by constructing grid boxes of a predefined size around the point of minimum MSLP for all cases within a category and averaging the desired NARR field within those boxes. The composite could then move with the storm because the composites were always centered on the surface low (the minimum MSLP grid-point) as the storm progressed. The grid box utilized was 109x109 grid points, which translates to 27.25 degrees length and width, an area that encompasses the entire eastern United States as well as a portion of Canada and the Gulf of Mexico. A representative map was added to the background of plots to give a sense of scale. As an example, Fig. 5.4 shows a composite of the 250 mb total wind for the classic cyclone cases.

#### **4.4 Snow Swath Composite**

To find differences in the observed snowfall among the cyclone categories, snow swath composites were created. As mentioned in Section 3.2, there was a major challenge associated with COOP daily snowfall measurements: non-uniform observation times (see Fig. 3.1, a histogram of observation times of snow for the CONUS for a given storm). As previously mentioned, the most ideal data would be consistent, hourly observations of snowfall amount; however, COOP stations only report once per day, and not all observations are taken the preferred 0700 observation time. This creates a situation wherein the observation might be taken during the snowfall or hours after the snow has already fallen. To compensate for this uncertainty and poor temporal resolution, composites were made of storm-total snow amounts, that is, the entirety of snow created by a storm while it exemplified a particular cyclone category.

To make the composites, the minimum MSLP grid points from the NARR composites were used. With the minimum MSLP at the beginning and ending of the storm period as the spatial window of interest, snowfall reports within  $3^\circ$  longitude on either side of the window were considered to be the snow swath for that storm. Plots of snow swath as determined by this method confirmed via swath shape that this method accurately captured most of the snowfall for which a particular case was responsible. One problem with this method was the fact that different storms were moving different directions, and so the resulting snow swath featured a tilt proportional to the direction of storm motion. Composites of these swaths were noisy due to the different swath angles. To correct this problem, the coordinate systems of the cases were rotated to the degree necessary to bring the storm motion to due easterly. This was accomplished by finding the average angle of storm motion relative to the east-west plane, which itself was accomplished by averaging the latitudinal and meridional distances the storm traveled through each 3-hour NARR time-step. After adjusting the coordinate systems, the snow swaths followed a general west-to east line, with slight deviations in the individual cases. The deviations were small enough that composites could then be performed on the snow swaths. An example snow-swath composite can be found in Fig. 5.23.

#### **4.5 Cross Sections**

To further analyze storm dynamics, composite cross sections of various thermodynamic fields were created. There are two ways to calculate composite cross sections: taking the composite of individual case cross sections, or compositing a field across the cases and then taking the cross section of that composite (in other words, the composite of a cross section versus the cross section of a composite). Both means were

used, and perhaps not surprisingly, both generated very similar results. The former method was selected for this study because it allowed for cross sections to be computed at locations tailored to the individual cases; this is in contrast with the latter method, which required a cross section to be made at only one location because it was a cross section of an already-composited field.

The cross sections were made at various angles through the cyclone, with the center of the surface low serving as the center of the cross section. The earlier method of composite hour selection was used again, with all the cross sections calculated at the middle hour (that is, the hour between storm formation and dissipation or relocation). To investigate the separated comma heads, two regions of interest were noted: the colder cloud-tops of the comma head, and the area of warmer cloud-tops between the comma head and the frontal zone, denoted the “clear air” area. Cross sections were computed through these areas by finding the angle from the east-west direction necessary to transect the area of interest. For many cases, these angles through the comma head and clear air were roughly perpendicular and parallel to the jet, respectively. Fig. 5.13 demonstrates the location of these cross-sectional lines for a representative separated comma-head case. Cross sections were also calculated on a north-south line, mostly for the computation of ageostrophic circulation following the ideas of Uccellini and Kocin (1987).

#### **4.6 Omega**

To analyze areas of rising motion within the cyclone cases, the quasi-geostrophic omega (hereafter referred to as QG omega) was calculated. The form of the QG omega

equation used in this study followed the work of Pauley and Nieman (1992), which used isobaric coordinates and separated the equation into four terms:

$$\text{(Eq. 4.1)} \quad \bar{\sigma} \nabla^2 \omega + f^2 \frac{\partial^2 \omega}{\partial p^2} = \nabla^2 (\vec{V}_g \cdot \nabla \alpha) + f \frac{\partial}{\partial p} \left[ \vec{V}_g \cdot \nabla (\zeta_g + f) \right], \text{ where } \sigma = -\frac{RT}{p\theta} \frac{\partial \theta}{\partial p},$$

$$\vec{V}_g \equiv \frac{1}{f} (\vec{k} \times \nabla \Phi), \quad \alpha = \frac{RT}{p}, \text{ and } \zeta_g = \frac{dv_g}{dx} - \frac{du_g}{dy} \text{ (see Wallace and Hobbs, pp. 48 and$$

376, and Holton, pp. 101 for definition of terms). The forcing for  $\omega$  is given by the terms of the right-hand side of Eq. 4.1. They are the Laplacian of geostrophic temperature advection and the vertical derivative of geostrophic vorticity advection respectively, and are hereafter referred to as the RHS (right-hand side).

Computation of QG omega required the compositing of the RHS first, followed by an iterative solving of the LHS (left-hand side). The complete RHS was composited individually for each case, and then omega was solved iteratively with the RHS as the forcing term. One-hundred iterations were sufficient for convergence to a solution for Eq. 4.1; iterations thereafter were found to yield little additional convergence. The resulting QG omega field was then composited and cross-sectioned in the same manner as the other model fields.

## 5. RESULTS

### 5.1 Thermodynamic Cause of Comma Head Separation

Extratropical cyclones responsible for heavy snow in the central and eastern United States were divided into three categories for this study: classic, separated, and warm separated. As detailed in Section 4.2, this classification refers to differing cloud-top temperatures among the various cases in the vicinity of the comma head, with the separation referring to an area of warmer clouds between the tip of the comma head and the frontal zone, leading to a visible discontinuity in infrared satellite imagery. To understand the thermodynamic differences among the three cases, analysis of many composited thermodynamic fields was performed. The majority of the resulting figures within this section are presented as four-panels, with the first three panels representing the three categories and the fourth panel containing the classic field subtracted from the separated comma-head field for the desired thermodynamic variable. In the case of plan view figures, a background of U.S. states is added to provide a sense of scale, and because the composite used a moving box centered about the minimum MSLP, the center of plan view figures always represents the surface low (an “L” is added to the fourth panel of these figures to represent the surface low location). Fig. 5.1 is a pictorial explanation of the plan view composites. For cross sections, the MSLP is marked on the horizontal axis with an L, with the other numbers representing the horizontal distance from the low, and the y-axis denoting vertical height in millibars. Positive values on the

y-axis reflect northward directions; this may represent northwest, north, or northeast directions depending on the cross-sectional angle. Fig. 5.2 explains the various components of the cross-sectional composites used in this study.

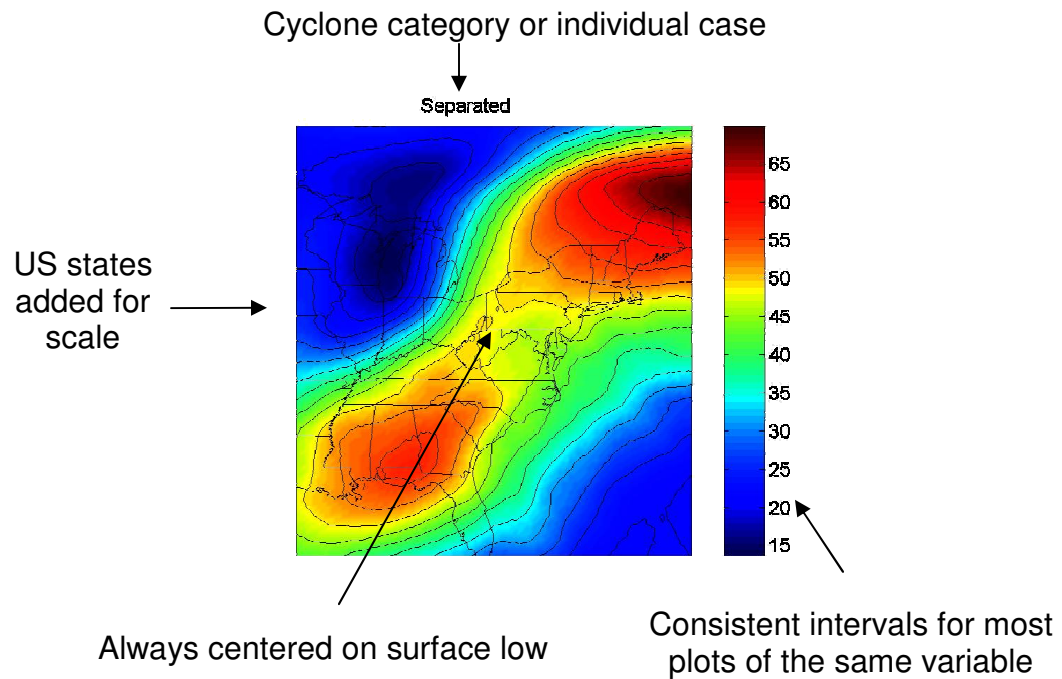


Fig. 5.1 – Explanation of the plan view composites

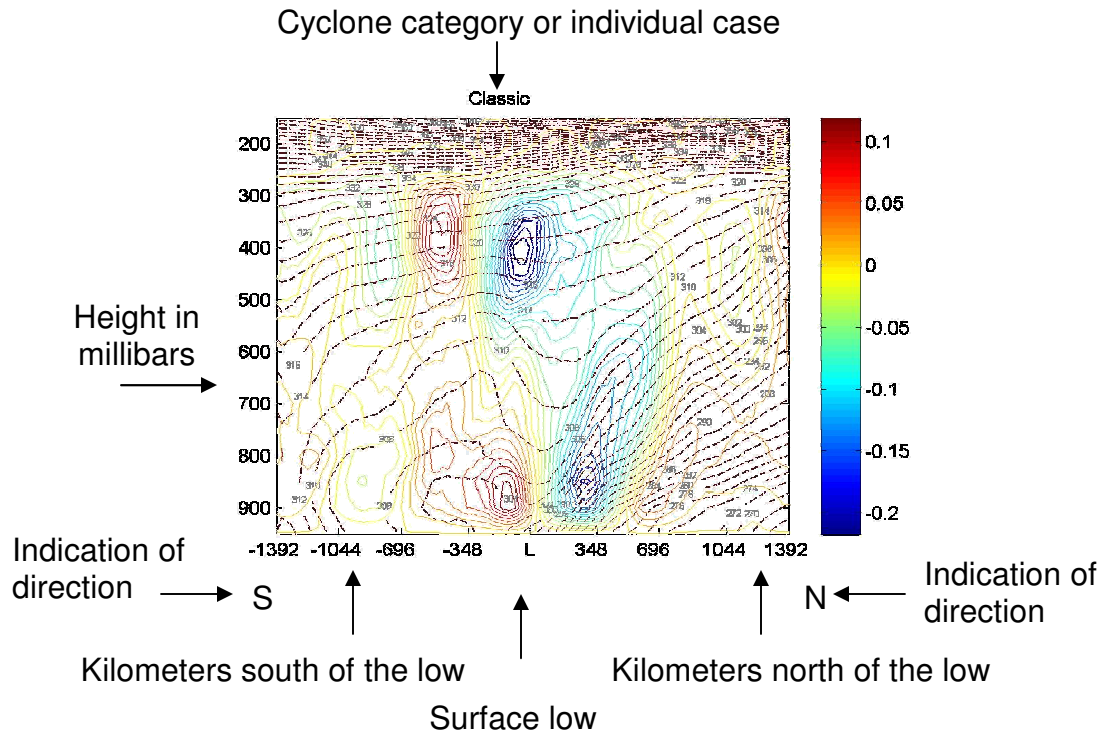


Fig. 5.2 – Explanation of the cross-sectional composites

In addition to composites, one case from each category was selected as a representative case for that category based on its exemplification of all this cases within that category: 17-Feb-2008 for the classic, 06-Feb-2008 for the separated, and 13-Mar-1999 for the warm separated. Plots of these individual cases are occasionally used in place of or along with the regular composites in situations where fine-scale features such as frontal zones would be smoothed out by compositing.

The most striking difference between the classic and separated comma-head cases was found in the wind fields, especially in the upper-troposphere. For the majority of the cases, the winds were found to reach a maximum at 250 mb (see Fig. 5.3), and so the winds at this level were designated as the jet. The composites of jet-level winds are shown in Fig. 5.4. The classic composite clearly shows a double-jet structure; that is, a southerly jet turning cyclonically to the right of the surface low, and a northerly jet lying

along the northern edge of the cyclone. Also of note is the manner in which the two jets intersect; the two jets are nearly perpendicular, with the entrance region of the northerly jet extending westward of the axis of the southerly jet. This jet structure is very similar to the cases analyzed by Uccellini (1987), wherein a double-jet structure created an enhanced updraft area. In contrast, the jet structures in the separated cases are much different. For both the separated and warm-separated cases, the jets are physically separated by a greater distance than the classic cases and oriented more parallel to each other, particularly for the separated comma-head category.

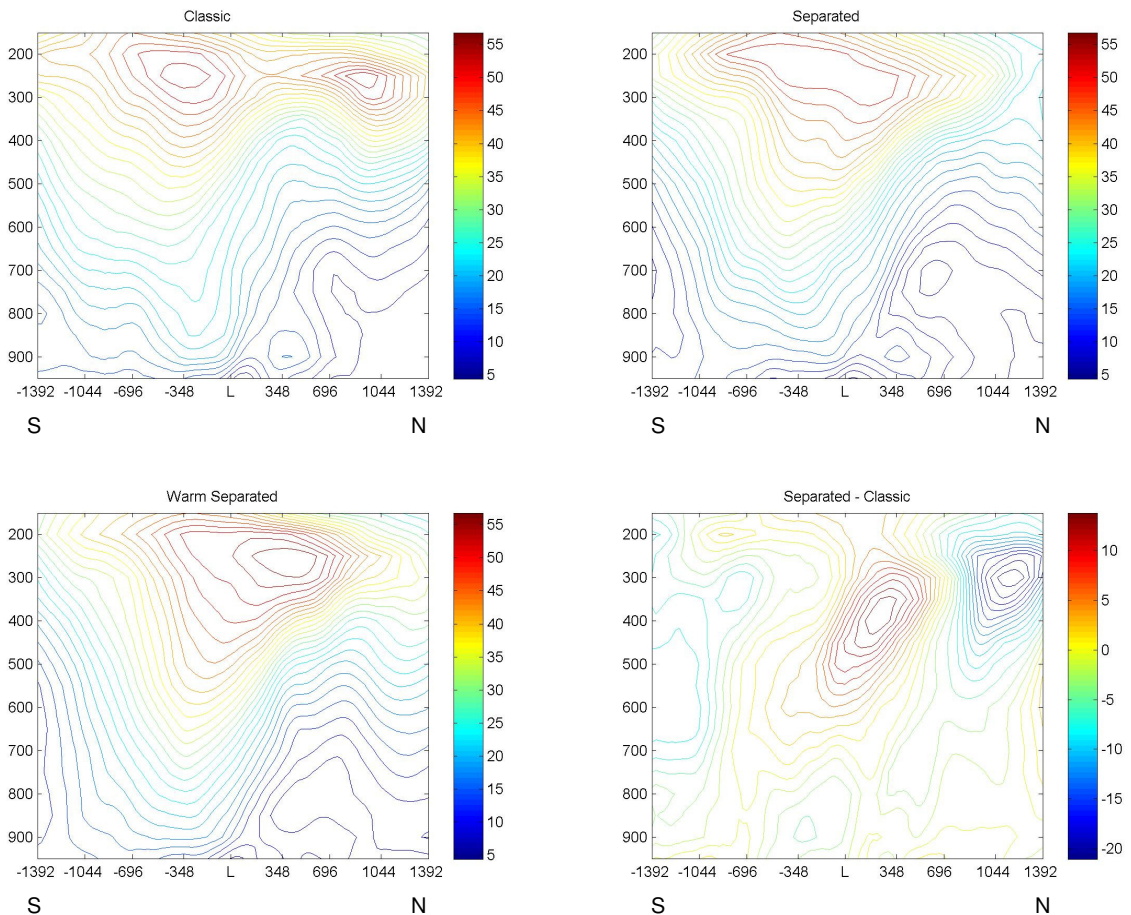


Fig. 5.3 – Cross-sectional composites of the total wind speed ( $\text{ms}^{-1}$ ) along a north-south line through the surface low. The y-axis is the height in hPa, and the x-axis is the distance from the surface low in km.

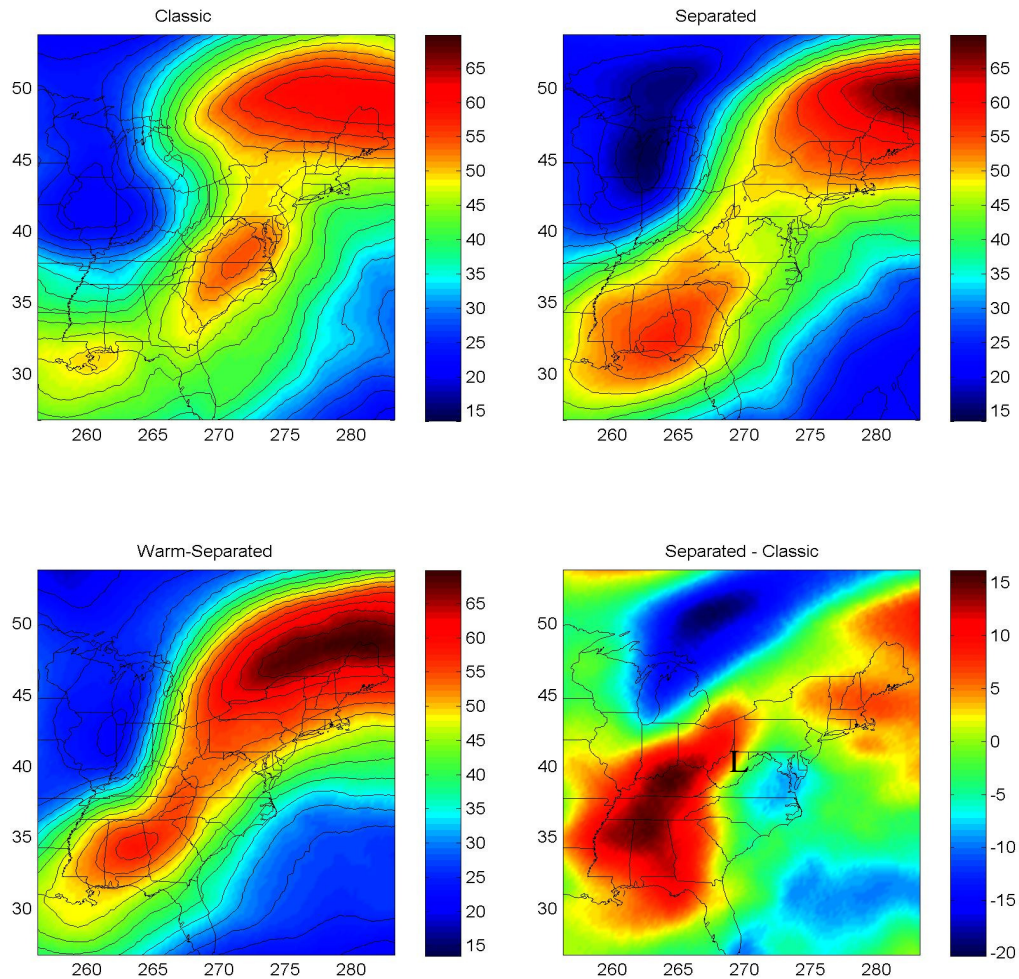


Fig. 5.4 – Composites of the upper-level jets (250 hPa winds in  $\text{ms}^{-1}$ ). The position of the surface low for each composite is indicated in the fourth panel. U.S. states are drawn to provide a sense of scale.

These jet orientations give insight to the observed cloud patterns of the categories (Uccellini et al., 1987). In the classic cases, the two jets are close enough to create a reinforced circulation to the north of the surface low, because the left exit of the southern jet and right entrance of the northern jet are nearly co-located. For the separated cases, the left exit region of the southern jet coincides with the location of the colder clouds of the comma head, the right entrance of the northern jet is in the vicinity of the northern side of the colder clouds of the frontal zone, and the area of warmer clouds in between (the disconnected area) lacks the enhanced circulation of the classic cases. The warm-

separated cases are similar, though the southern jet is less distinctive, possibly explaining the warmer cloud-tops in comparison to the separated cases. Furthermore, the two jets are closer in the warm-separated cases, which is probably associated with the fact that the degree of separation (that is, the distance between the colder clouds of the comma head and the frontal zone) is less for the warm-separated cases than the separated cases.

Fig. 5.5 shows the jets again, this time for the representative cases. The jets of the classic case are about 600 km apart, whereas they are nearly 1000 km apart for the separated and warm-separated cases. The southern jet appears much weaker in the classic case, but closer inspection shows that the southern jet is merely stronger at a lower height for this case. Comparing the separated case composite to the companion satellite imagery (all the cases in Table 4.2) reveals that the left-exit region of the southern jet lines up with the location of the colder clouds of the comma head, while the right-entrance region of the northern jet is on the northern side of the frontal-zone cloud band. The southern jet of the warm-separated representative case is weak, possibly explaining the warmer cloud tops in comparison to the separated composite and implied weaker vertical motion in the comma head for this case.

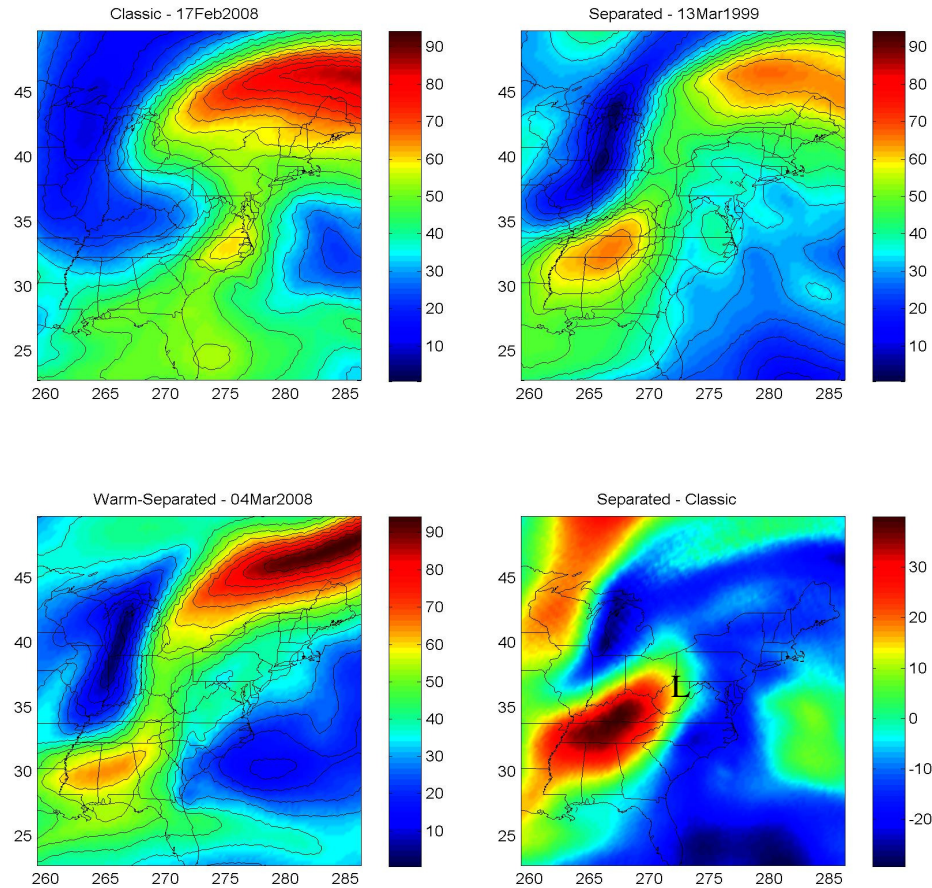


Fig. 5.5 – Upper-level jets ( $250 \text{ hPa}$  winds in  $\text{ms}^{-1}$ ) for the representative cases.

Another thermodynamic field commonly associated with cyclone development is geopotential heights (Young, 1993). Fig. 5.6 is a composite of  $500 \text{ mb}$  heights for the three cyclone categories. Because the point of minimum MSLP is fixed at the center of the grid boxes, it is apparent that the classic cases are more vertically stacked (a condition wherein the center of the upper-level low is co-located with the center the surface low) than the separated cases. Another feature of note is the closed isoline of geopotential height found with the separated composite; this feature is absent in the classic composite, while the warm-separated is in between the two with a nearly closed contour. The classic cases have a negatively-tilted trough, the separated cases have a slightly-positive tilted

rough, and the warm-separated cases are neutral. The negative tilt of the classic composite, combined with the asymmetrical southward bulge of contours hints at the presence of a shortwave trough moving through the broader longwave trough (Section 5.2 notes similarities of this concept to Young, 1993).

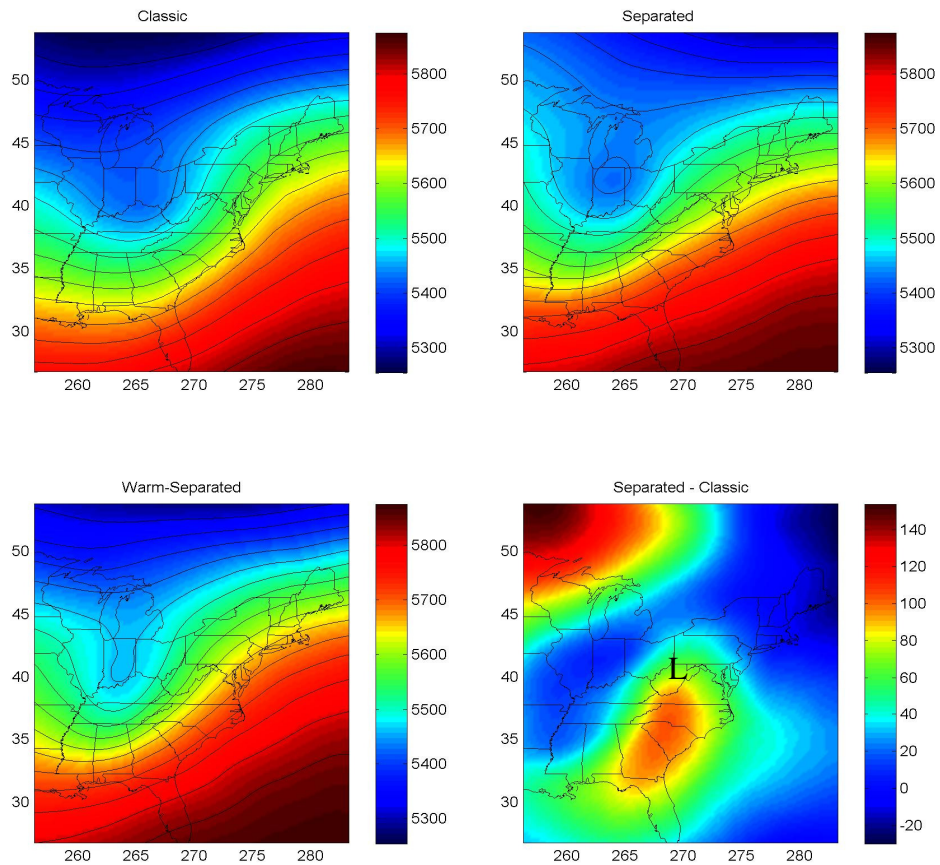


Fig. 5.6 – Composite 500 hPa geopotential heights (gpm).

Martin (1999) noted the trowal airstream (rapid cyclonic ascent of warm-sector air within a cyclone) as being the primary cause of clouds and precipitation within the comma head. Thus, Martin associated the appearance of a trowal with development of comma heads. As detailed in Section 2.1, a trowal is an area of warm air aloft which wraps cyclonically around the low, overruns the cooler air of the cold front, and is thus usually associated with the occlusion process. Following Martin, trowals can be located

by analyzing plan views of  $\theta_e$  (equivalent potential temperature) at lower to middle levels of the troposphere, and noting a westward extension of high  $\theta_e$  values to the north of the low. Fig. 5.7 is a plan view of  $\theta_e$  at 750 mb for composites of the three cyclone categories. A modest westward extension of warmer  $\theta_e$  air is visible to the north and west of the surface low (which is again at the center of the image) for the composite of the classic cases, hinting at the existence of a trowal. While there is also some cyclonic turning of the warmer  $\theta_e$  contours for the warm-separated cases and to a lesser degree the separated cases, it is most prominent for the classic cases.

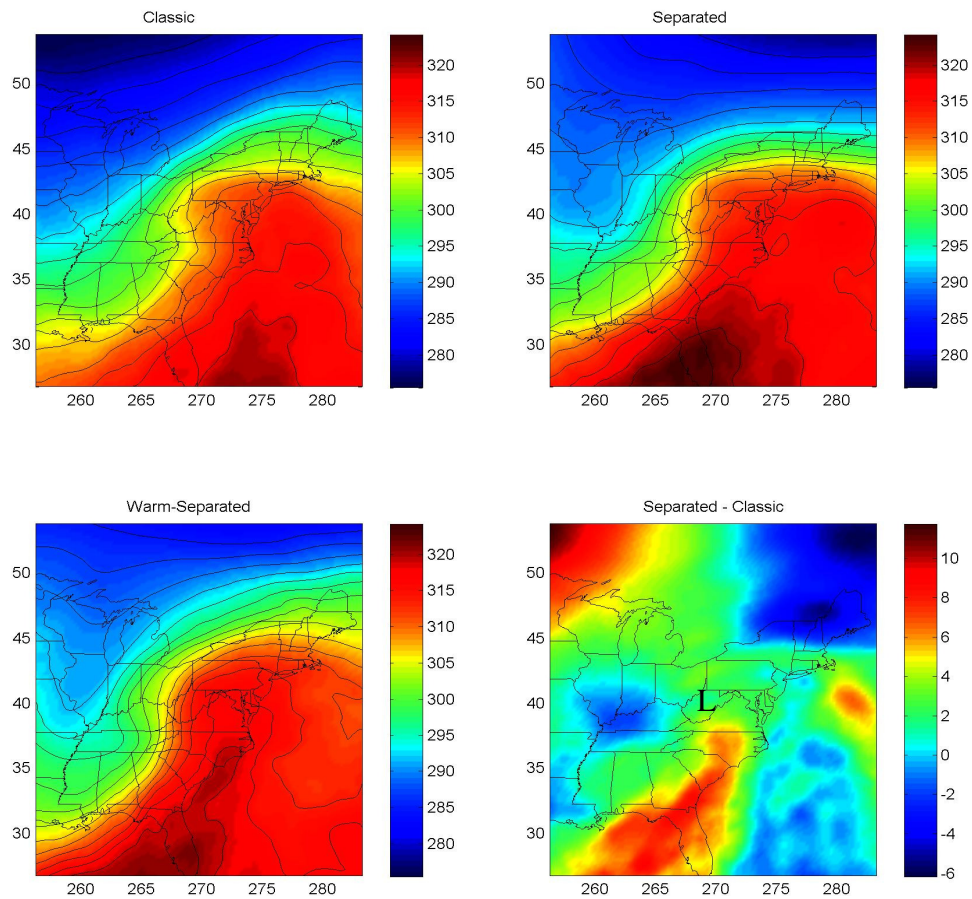


Fig. 5.7 – Composite equivalent potential temperature (K) at 750 hPa.

Because the trowal is a relatively fine-scale feature, some of its detail is smoothed out in the compositing process. Fig. 5.8 is the same plan view as Fig. 5.7, with the

representative cases plotted in place of the composites. The trowal is much more evident for the classic case in this figure. Specifically, the westward extension of warmer  $\theta_e$  contours near the surface low extend over 500 km westward, a definitive trowal signature as defined by Martin. The warm-separated case exhibits a trowal-like structure, although the westward extent is minimal. In contrast, the separated case shows no organized trowal structure. Thus, the plan view plots indicate that a trowal is present in the representative classic case, possibly present in the warm-separated case, and absent in the separated case.

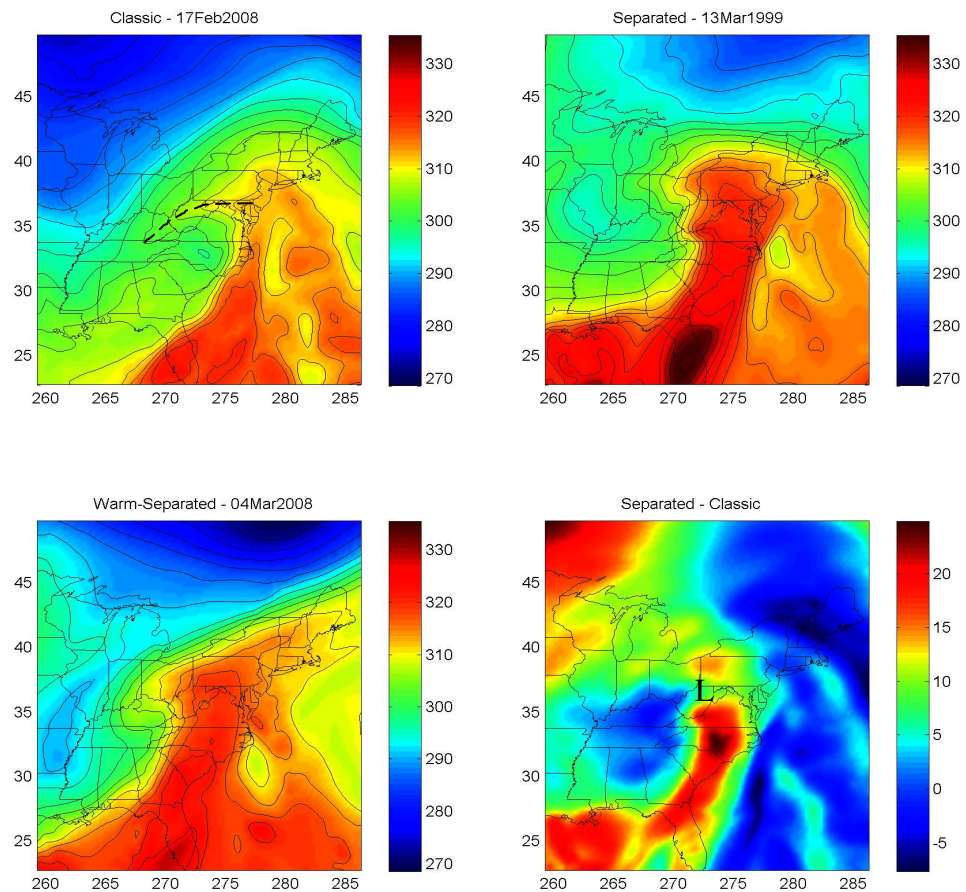


Fig. 5.8 – Equivalent potential temperature (K) at 750 hPa for the representative cases. The dashed line for the classic case represents the trowal location.

According to Martin (1999), one feature associated with trowal development within an extratropical cyclone is a treble-clef-shaped potential vorticity anomaly, so called because it is similar to the bottom part of a treble clef (although backwards). Martin found this to be a common feature among systems exhibiting a trowal. Fig. 5.9 is a plan view of Ertel Potential Vorticity calculated at 300 mb for the representative cases. The classic case exemplifies the treble clef shape as described by Martin, while the warm separated case could be thought of as a developing treble clef, and the separated case shows a completely different shape. This agrees with the earlier finding of classic cases featuring trowals, warm separated cases showing weak or developing trowals, and separated cases having no trowal.

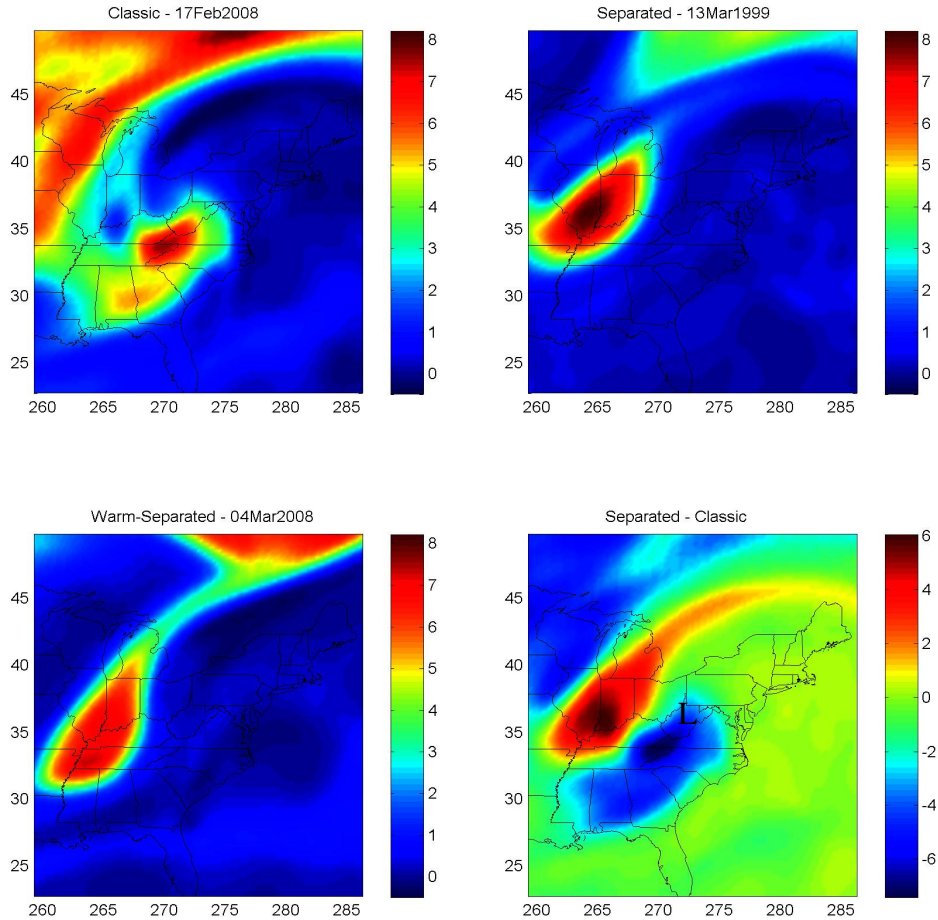


Fig. 5.9 – Ertel potential vorticity in PV units ( $1.0 \times 10^{-6} \text{ m}^2 \text{ s}^{-1} \text{ K kg}^{-1}$ ) at 350 hPa for the representative cases.

The trowal concept can be related to the earlier topic of jet streak position via the thermal wind equation. This equation implies that the vertical derivative of geostrophic wind speed is proportional to the horizontal gradient of temperature, as shown in the

following approximated form: Eq. 5.1  $\frac{\partial u_g}{\partial z} \approx \frac{-g}{f\theta} \frac{\partial \theta}{\partial y}$  (potential temperature is substituted

for temperature and the other variables represent the same parameters as in Eq. 4.1). It should be noted that use of Eq. 5.1 for meridional cross sections as in done in the following figure requires the zonal wind approximation, that is, it assumes that the total wind is composed entirely of the “u” component. The existence of a trowal implies a

weaker thermal gradient in the vertical because the area of warmer air aloft causes lines of potential temperature to begin to flatten and even overturn (a “valley” shape) in the vertical; both these shapes of  $\theta$  represent a decrease in its horizontal gradient. By the thermal wind argument, this decrease in the horizontal gradient of temperature must be associated with a weakening of the vertical derivative of geostrophic wind. This decreased derivative of vertical wind is manifested in the classic cases as a minimum in wind speed between two jets, as shown in a cross section in Fig. 5.10. Following the  $\theta$  lines for the classic composite within the 500-600 mb layer reveals an area of weak horizontal  $\theta$  gradient from about 300 km south to 300 km north of the surface low (boxed area in Fig. 5.8). This area is aligned with the area of weaker vertical wind shear mentioned earlier between the two jets. In contrast, the separated and warm separated composites have a nearly constant horizontal gradient of  $\theta$  in the 500-600 mb layer and strong vertical wind shear. Therefore, the trough position and jet positions appear to be dynamically connected, although it is unclear which feature causes the other, if at all (the causality of one feature over the other is beyond the scope of this research).

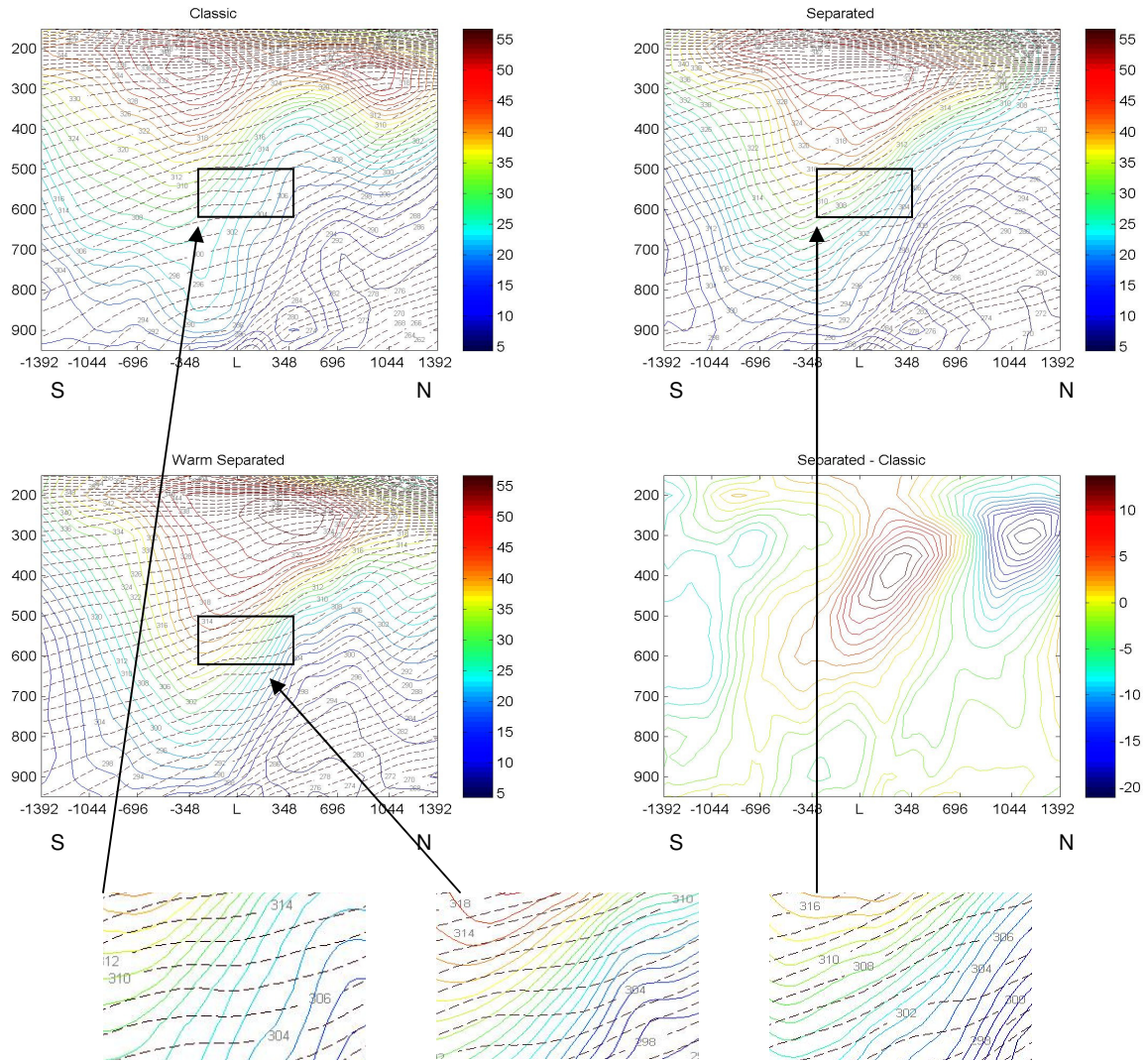


Fig. 5.10 – Cross-sectional composites of total wind speed ( $\text{ms}^{-1}$ ) overlaid with potential temperature (K) along a north-south line through the surface low. The boxed region is the area discussed in the previous paragraph and is enlarged beneath the figure. The axes represent the same variables as in Fig. 5.3.

As before, the representative cases can be used to better analyze the smaller thermodynamic structures, and so Fig. 5.11 provides the same plot as 5.10 with the representative cases swapped for the composites. For the representative classic case, the weakened horizontal thermal gradient is manifested as a “valley” shape in the  $\theta$  contours (boxed region in Fig. 5.11), and as would be expected from the thermal wind argument, there is an associated minimum in geostrophic wind directly above. Meanwhile, the

separated and warm separated representative cases show a nearly constant horizontal gradient of theta, and an associated strong vertical gradient of geostrophic wind.

Therefore, via the thermal wind equation, the appearance of a trowal for the classic cases is at least partially associated with the upper-level jet positions.

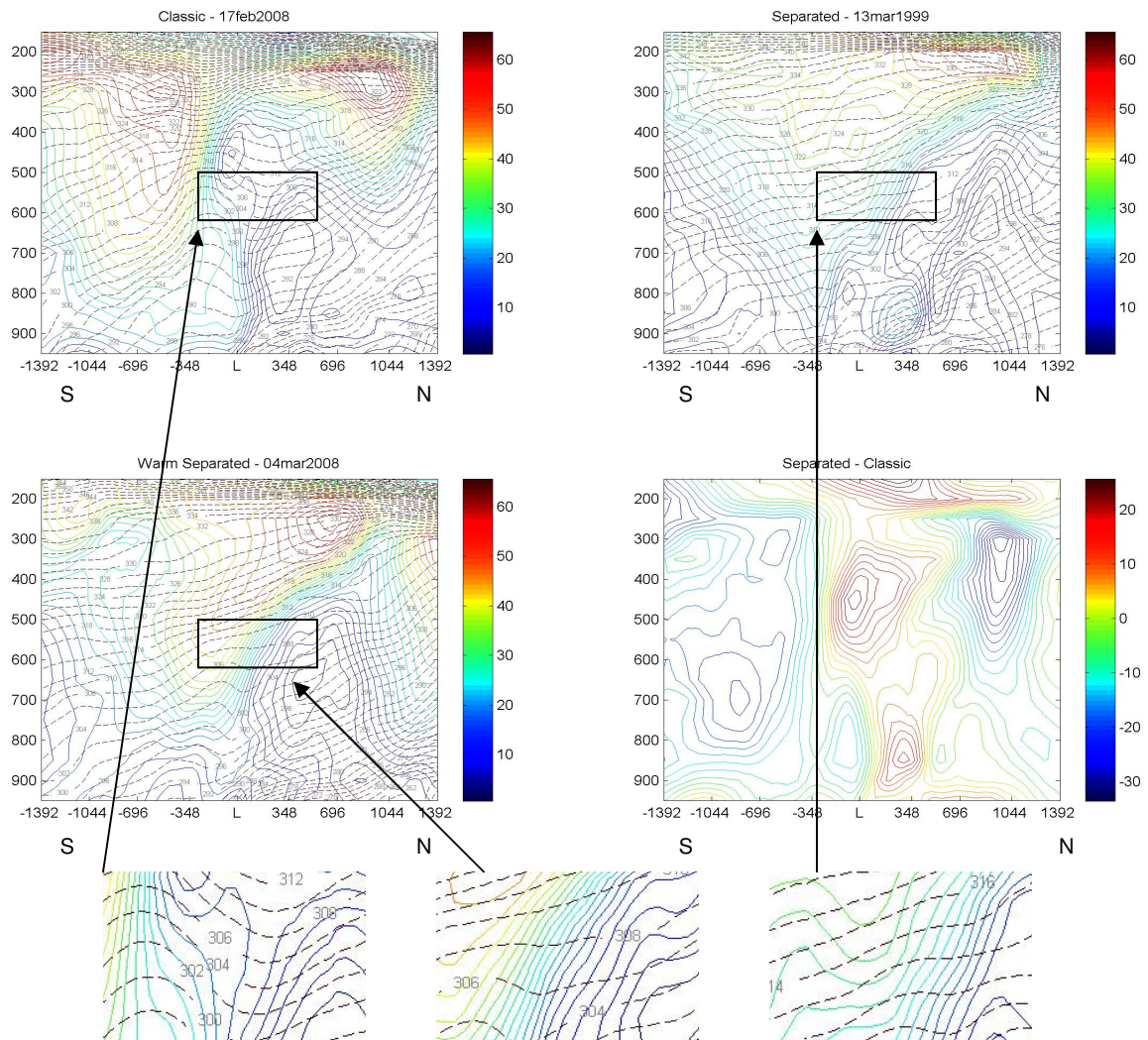


Fig. 5.11 – Cross sections for the representative cases of total wind speed ( $\text{ms}^{-1}$ ) overlaid with potential temperature (K) along a north-south line through the surface low. The boxed region is the area discussed in the previous paragraph and is enlarged beneath the figure. The axes represent the same variables as in Fig. 5.3.

The vertical broadening of  $\theta$  lines within a trowal creates a condition of reduced static stability, which can be represented as the vertical derivative of theta. When the change of

$\theta$  in the vertical is positive, the atmosphere is statically stable; when it is negative, the environment is statically unstable. Thus, the areas around the low analyzed as trowals for Figures 5.10 and 5.11 represent areas of reduced static stability, because the trowal in both plots is an area of decreased vertical gradient of theta. This coincides with Martin's (1998) notion of the trowal airstream being associated with clouds and precipitation, because convection is more likely in an area of reduced stability.

Quasi-geostrophic omega (vertical motion) was calculated for all the cases using Eq. 4.1 as detailed in Section 4.6. There are three key areas of interest for analyzing the omega fields in this study: the area north of the surface low, the area of colder cloud-tops within the comma head, and the "clear air" region of warmer clouds between the comma head and the frontal zone. For each of the separated and warm-separated cases, angles relative to the east-west direction were found such that the cross-sectional line would transect the comma head and clear-air regions, respectively. Because neither of these spatial designations applied to the classic cases (recall that the classic cases do not have a discontinuity between the comma head and frontal zone), the comma head and clear-air angles of the separated cases were averaged and then applied to the classic cases. These average angles were  $70^\circ$  for the clear-air region, and  $130^\circ$  for the comma-head region, roughly corresponding to directions parallel and perpendicular to the mean jet axis. Figures 5.12 through 5.14 show these cross-sectional lines applied to the three representative cases.

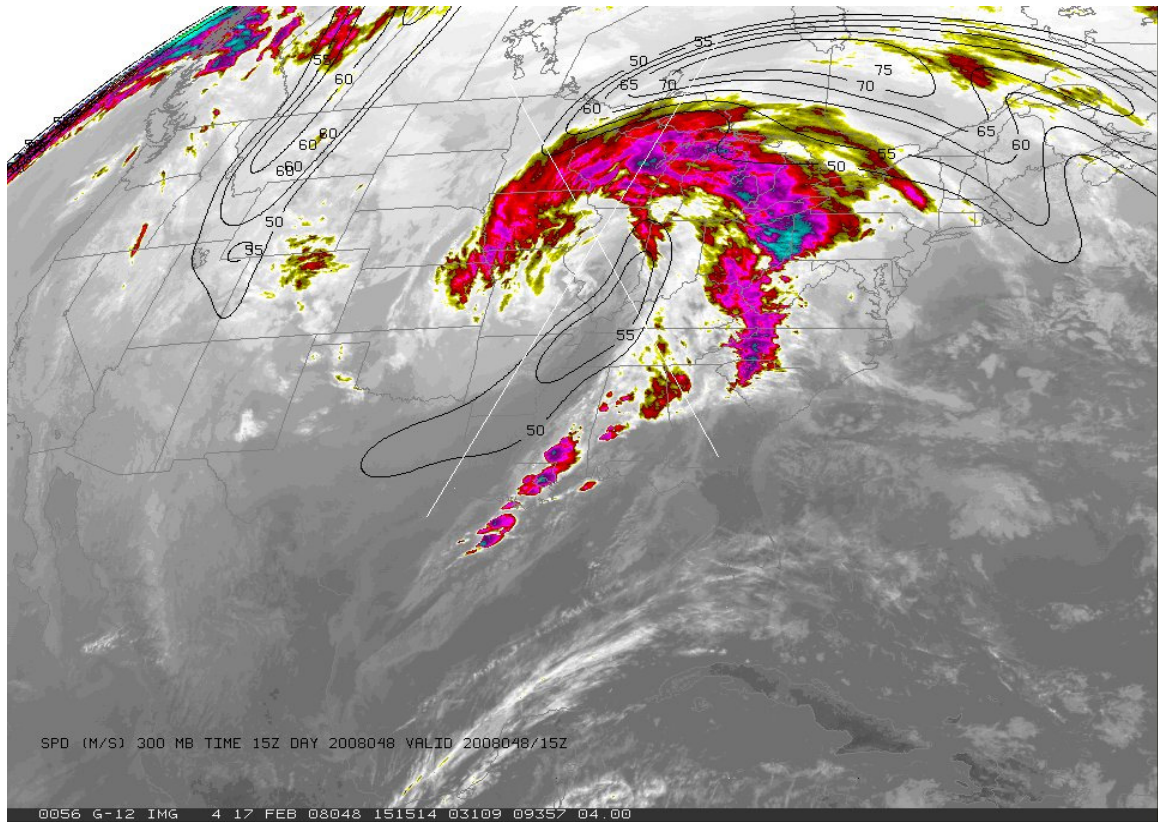


Fig. 5.12 – 10.7  $\mu\text{m}$  satellite imagery for 17 Feb. 2008 at 15:15 Z, as classic case. The cross-sectional directions are indicated by the white lines, with the positively-sloped line representing the clear-air direction, and the other indicating the comma-head direction. The black contours are the jets, which represent the total wind at 250 hPa contoured from  $50 \text{ m s}^{-1}$  and above.

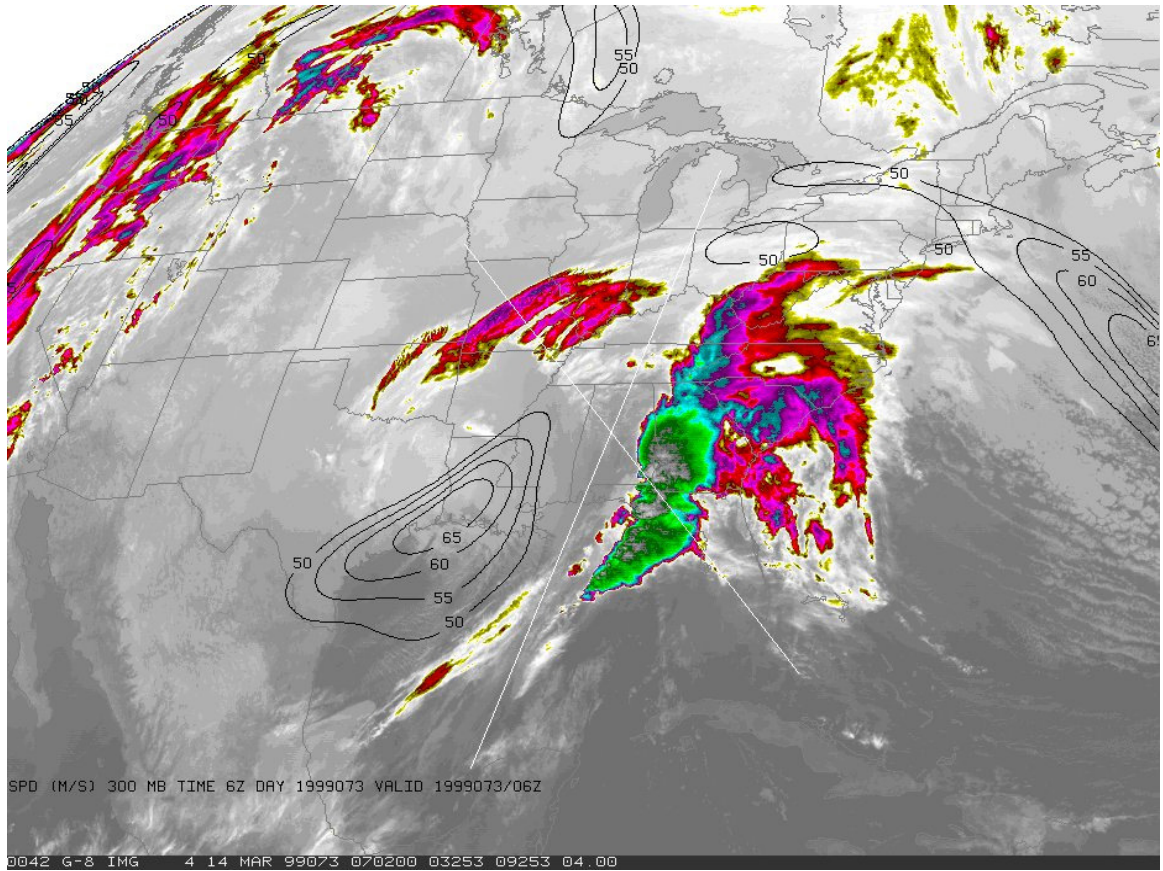


Fig. 5.13 – As in Fig. 5.12, except for the representative separated case.

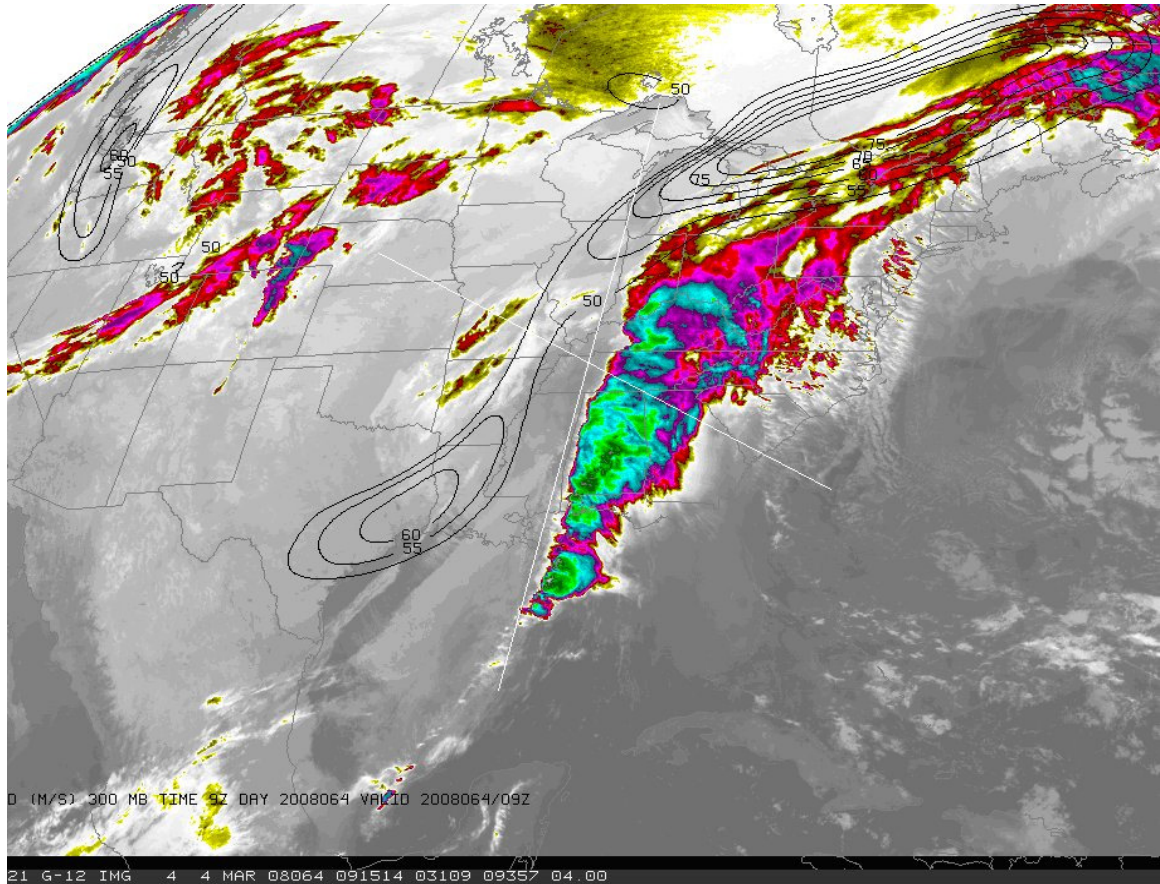


Fig. 5.14 – As in Fig. 5.12, except for the representative warm-separated case.

A composite cross section of omega along a line from north to south is shown in Fig. 5.15, with dashed contours of  $\theta_e$  overlaid. As before, the first three panels represent the classic, separated, and warm separated, while the fourth panel is the classic field subtracted from the separated field. The omega contours are colored such that an omega of zero is always the same color within a figure, while blues represent rising motion and reds represent sinking motion. All three cases show a maximum in upward motion north of the surface low from 900 to 700 mb, which is associated with the low-level frontal zone in that area as evidenced by the tightly-packed  $\theta_e$  contours. One feature of note is the broad area of rising motion within the classic case above and to the north of the surface low, which is absent within the separated composite and nearly absent in the

warm-separated composite. This area is associated with a dip in the  $\theta_e$  contours above the low, which is a manifestation of the trowal. Thus, the trowal airstream (as denoted by Martin) is most likely associated with the broad area of rising motion within the classic composite, and its absence is probably connected with the lack of rising motion in the same area for both of the separated composites.

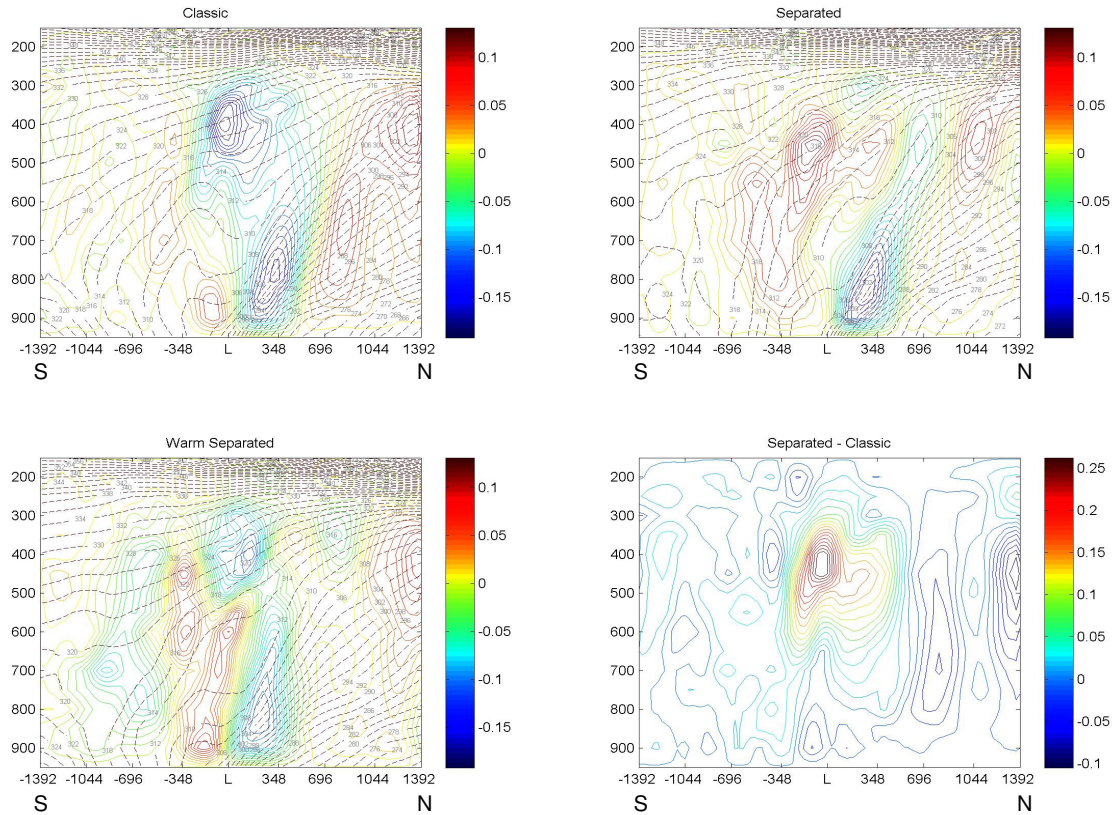


Fig. 5.15 – Cross-sectional composites of omega ( $\text{Pa s}^{-1}$ ) overlaid with equivalent potential temperature (K) along a north-south line through the surface low. The axes represent the same variables as in Fig. 5.3.

Fig. 5.16 shows omega along a cross section through the comma head for the composites, with wind speeds dashed and overlaid. One feature which is immediately apparent is the strong updraft within the separated case centered at 400 mb about 550 km northwest of the low. Analysis of the wind contours reveals that this maximum is associated with the northern edge of the southern jet, which indicates that the highest

clouds of the comma head are a result of rising motion from the left exit of the southern jet. Further confirmation of this idea is provided by the difference plot, which clearly indicates an omega couplet associated with a jet core (boxed area in Fig. 5.16), which is in this case the position of the southern jet.

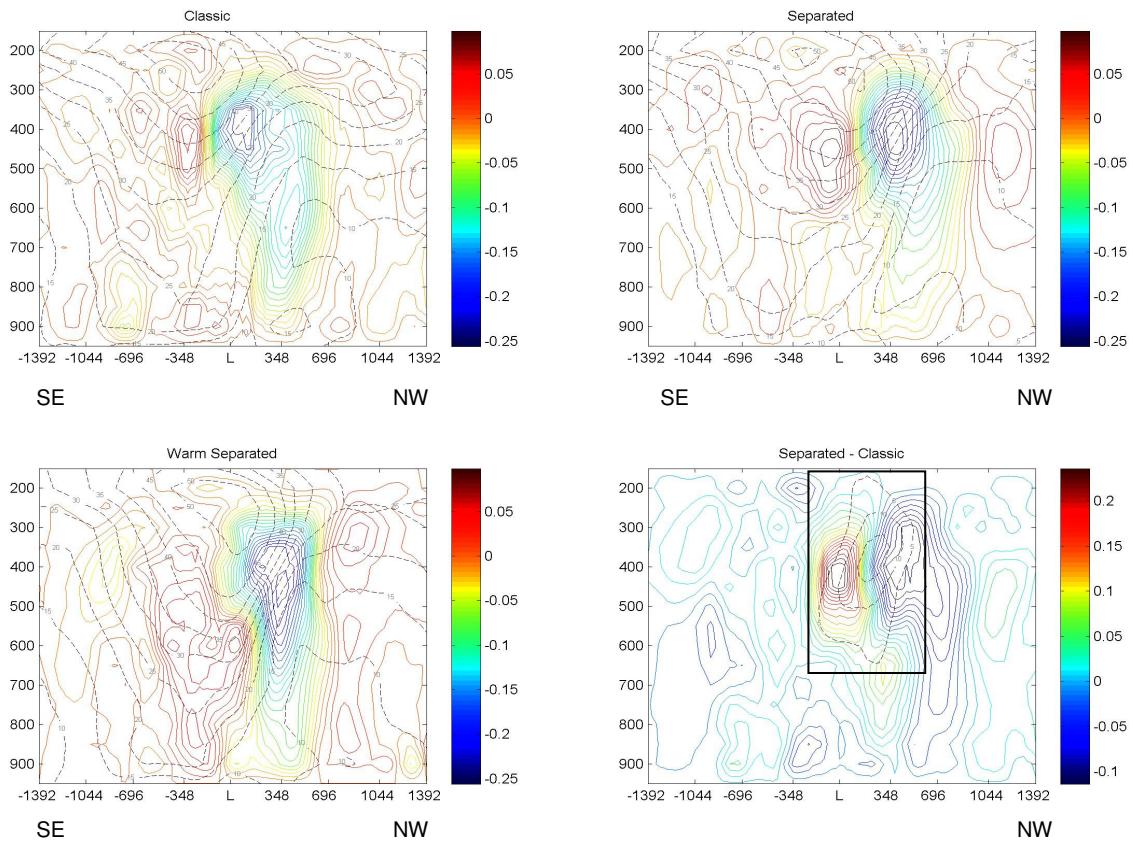


Fig. 5.16 – Cross-sectional composites of omega ( $\text{Pa s}^{-1}$ ) overlaid with total wind speed ( $\text{ms}^{-1}$ ) along a line through the comma head. The boxed region is the area discussed in the previous paragraph. The axes represent the same variables as in Fig. 5.3.

Fig. 5.17 is a plot of omega with  $\theta_e$  overlaid, this time along a line through the “clear air” area of the cases. Once again, a trowal is evident in the classic composite, absent in the separated composite, and nearly absent in the warm separated, while the trowal is located in the vicinity of an area of widespread rising motion. However, the separated composite now shows rising motion extending to only about 600 mb, with sinking motion above, which is consistent with the fact that the separated cases had no high clouds in this

area. The rising motion of the southern jet is not as apparent as before because this cross-sectional direction is parallel to the jet direction (the cross section must be perpendicular to the jet axis to fully capture the associated rising motion). The classic case, meanwhile, is still showing rising motion in this area, probably from the circulation of the northern jet. Thus, the absence of a trough airstream means that it is unable to provide widespread rising motion in mid-levels, and the lack of a circulation from the southern jet means that it cannot drive the formation of clouds in the upper-troposphere for the separated cases.

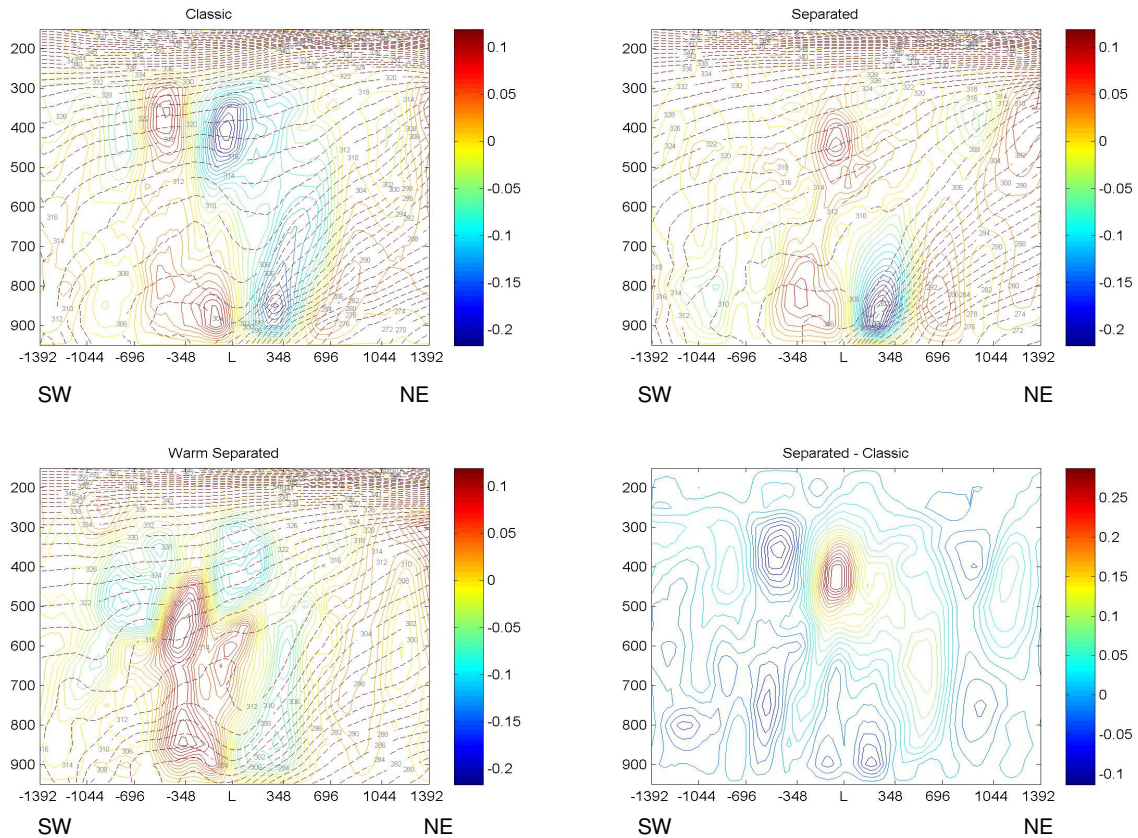


Fig. 5.17 – Cross-sectional composites of omega ( $\text{Pa s}^{-1}$ ) overlaid with equivalent potential temperature (K) along a line through the clear air area. The axes represent the same variables as in Fig. 5.3.

Following Uccellini and Kocin (1987), jet circulations can be analyzed by creating a cross section of ageostrophic circulations composed of ageostrophic winds tangential to the plane of the cross section and  $\omega$ . Using this method, they were able to diagnose both

thermally direct and indirect jet circulations by over-plotting  $\theta$ ; they were also able to locate a slanted updraft in between the circulations. Fig. 5.18 is an example of this technique applied to the cases of this study. The cross section is taken along a north-south line, and so the horizontal component of the circulation is the  $v$ -component of the ageostrophic wind, with positive values of  $v$  translating to rightward directions in this figure. The vertical component is  $\omega$  as calculated earlier, with a scaling factor applied to assist with visualization. Potential temperature is dashed over the ageostrophic circulation arrows to indicate whether the circulation is direct or indirect; these are marked as “D” and “I” respectively. Fig. 5.19 shows the cross sections relative to the jet positions in order to demonstrate visually which jets are associated with which circulations. The classic case composite shows both the direct and indirect circulations, with the direct circulation being particularly distinct to the north (rightward in this figure) of the low. The separated cases, however, do not show these circulations as distinctly. While the direct circulation is apparent, the indirect circulation is not very organized. Although an apparent circulation exists in the vicinity of the expected indirect circulation, the center of this circulation is around 850 mb, which is too low for it to be a result of the jet circulations. Additionally, while the slantwise core of upward motion extends up to 300 mb for the classic composite, the corresponding core of the separated composite is vertically inhibited by sinking motion around 550 mb, a possible result of these cases lacking the reinforcing action of two jet circulations. Meanwhile, the warm separated cases lack the direct circulation entirely, with a low-level circulation in the vicinity of the expected indirect circulation in a manner similar to the separated cases. Once again, the

lack of the reinforcing double jet structure could be preventing the slantwise updraft from rising above 550 mb.

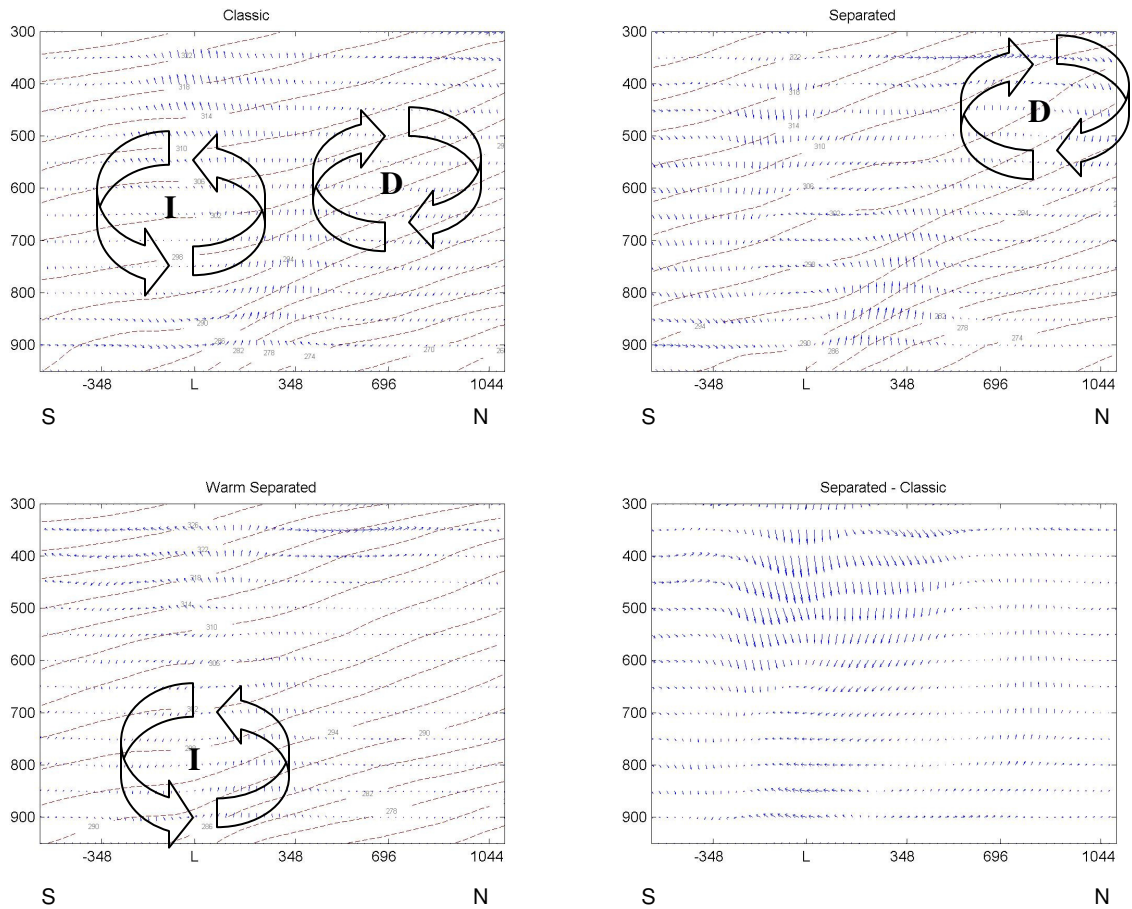


Fig. 5.18 – Vector representations of omega and the v-components of the ageostrophic wind in a cross section along a north-south line through the surface low. The circulations mentioned in the preceding text are represented by arrows; D and I denote direct and indirect circulations, respectively. Potential temperature is dashed every 4 K. The axes represent the same variables as in Fig. 5.1.

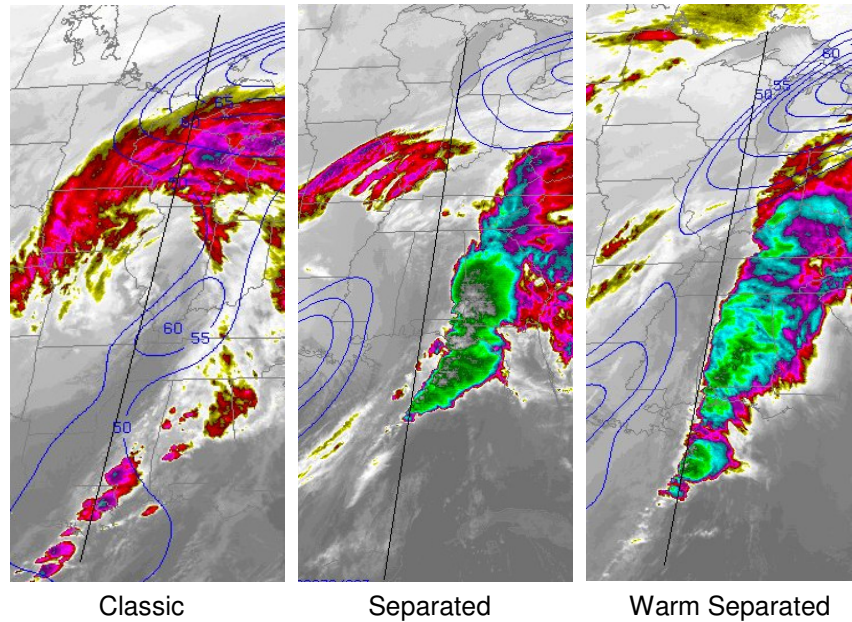


Fig. 5.19 – Images depicting the cross section location of Fig. 5.18 relative to the jets. The jets are contoured every  $5 \text{ ms}^{-1}$  above  $50 \text{ ms}^{-1}$ .

Figures 5.20 through 5.22 are conceptual models of the three cyclone categories featuring the pertinent dynamic features mentioned earlier. These figures show the average positions of the colder clouds (brightness temperatures less than  $250 \text{ K}$ ), the jets ( $250 \text{ mb}$  winds greater than  $50 \text{ m/s}$ ), the ageostrophic circulations induced by the jets, and the location of the surface snow swath relative to the comma head. The trowal airstream is indicated in the classic model only, because it is the only category which contains that feature. The key points which are illustrated in these figures are the jet position and associated circulations relative to the cloud field, and the existence of a trowal. In the classic example, the ageostrophic circulations of the jets are positioned in a reinforcing manner in the vicinity of the snow swath, as opposed to separated and warm-separated examples wherein the circulations of the two jets are isolated from each other. Additionally, the classic case features a trowal airstream which provides additional

instability in the vicinity of the snow swath, while this feature is absent for both the separated and warm-separated categories.

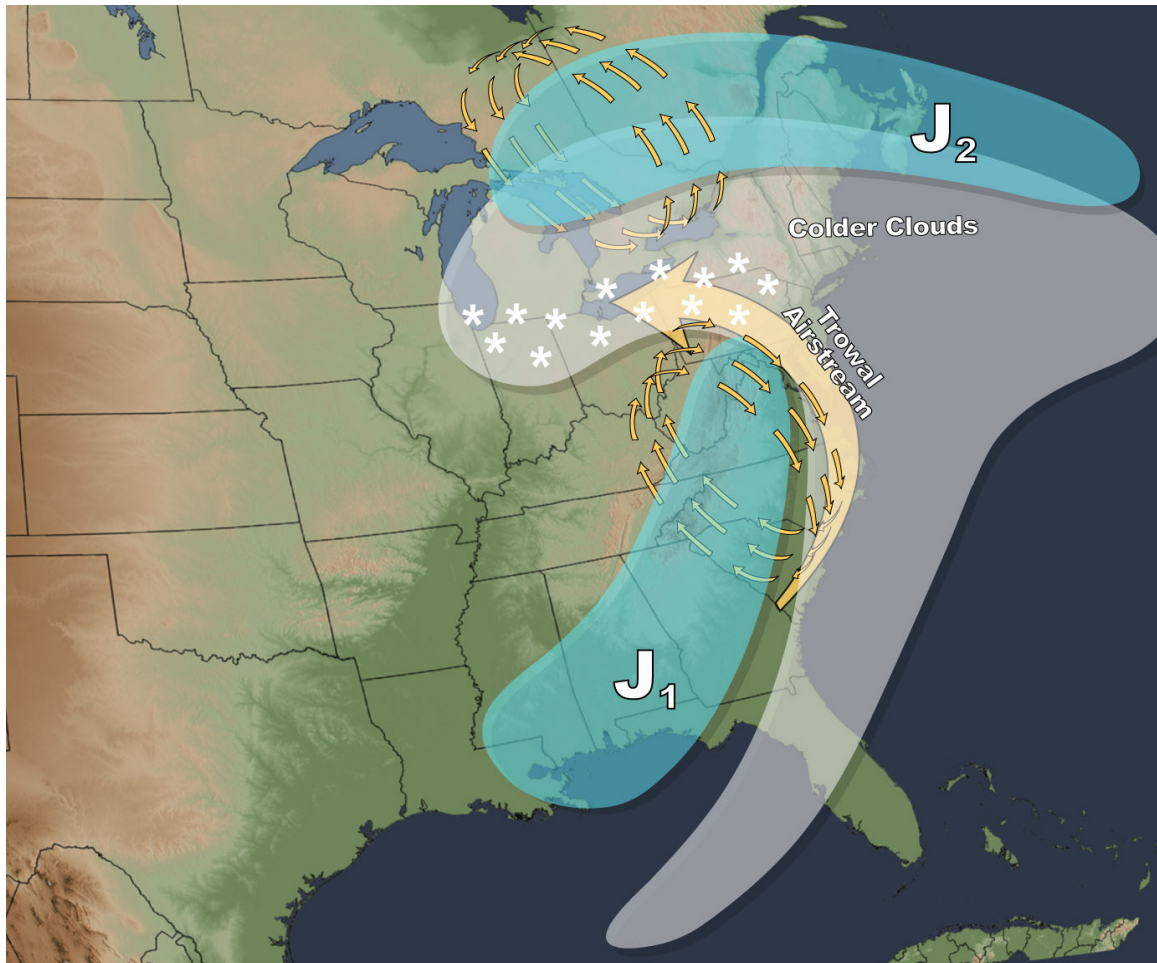


Fig. 5.20 – Conceptual model of the classic cases. J<sub>1</sub> is the southern jet (250 hPa winds greater than  $50 \text{ ms}^{-1}$ ) and J<sub>2</sub> is the northern; the arrows represent the ageostrophic circulations caused by the jets. The colder clouds (brightness temperatures less than 250 K) are represented as the grey area. The location and shape of the surface snow swath is approximated by the white asterisks. The approximate trowal airstream location is represented by the yellow arrow.

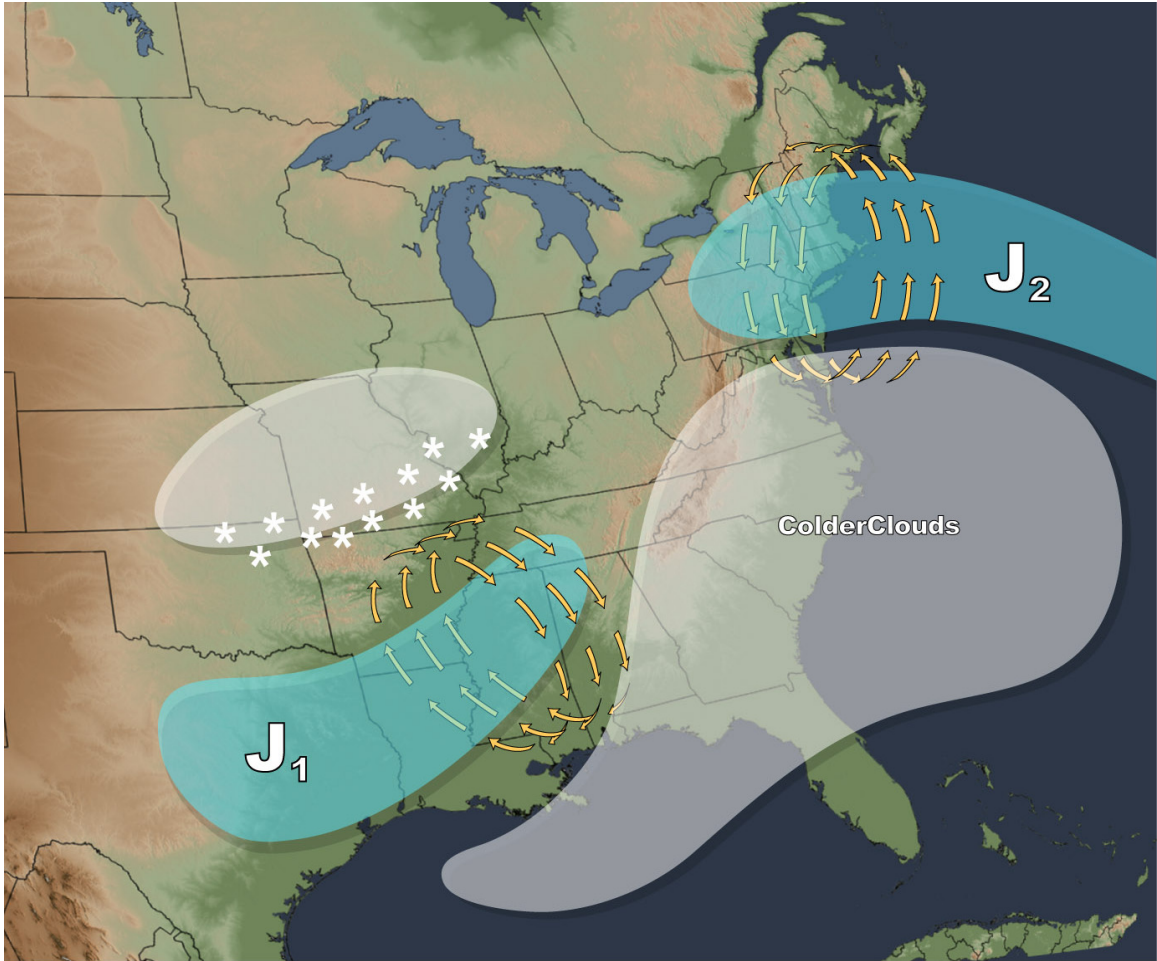


Fig. 5.21 – As in Fig. 5.20, except for the separated category.

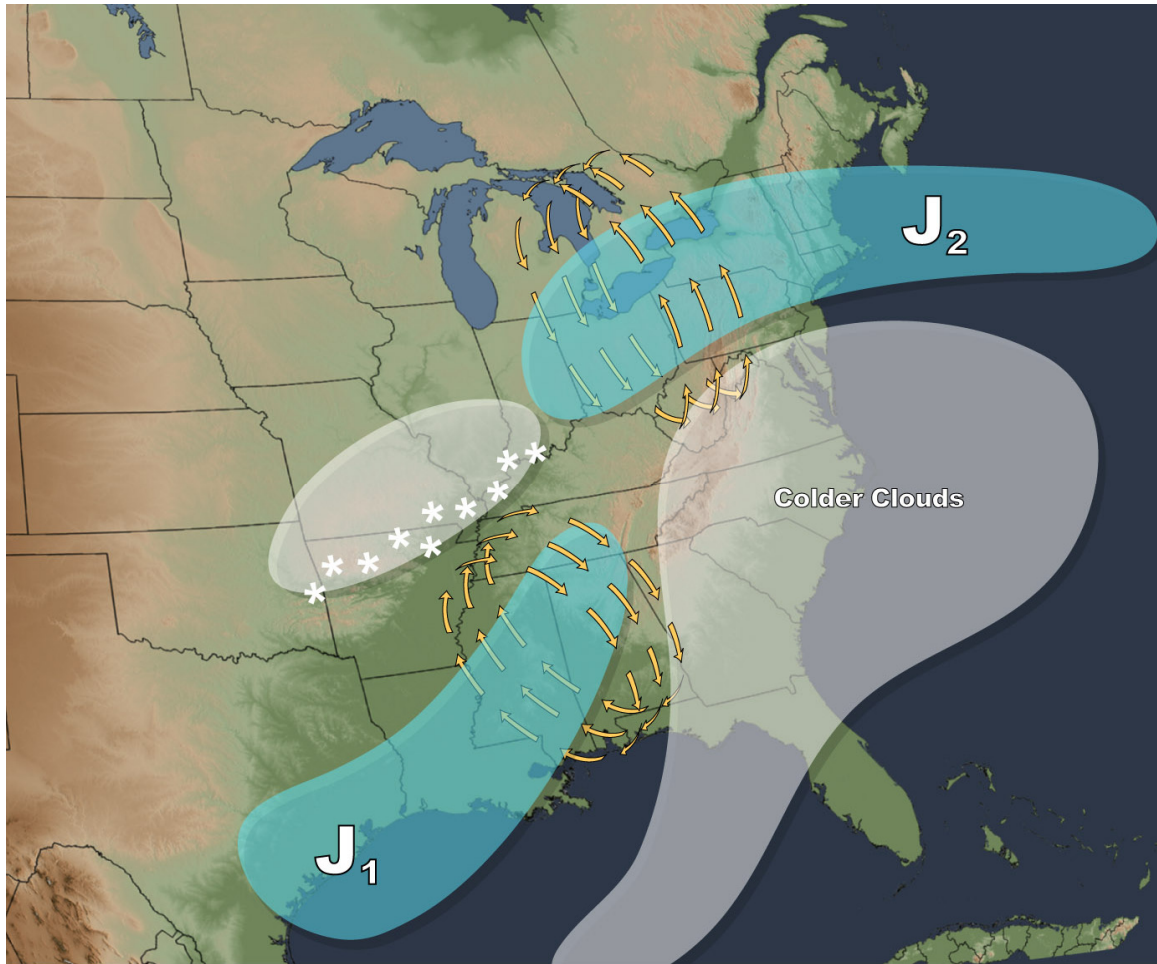


Fig. 5.22 – As in Fig. 5.20, except for the warm-separated category.

## 5.2 Comparison of the Present Cyclone Classification to Previous Studies

As discussed in Section 2.1, there has been a lot of previous work on classifying extratropical cyclones. One major difference between this present study and the three papers mentioned in Section 2.1 is that this study focused on cyclones in a relatively limited geographical area, specifically the area of the United States east of the Rocky Mountains and west of the Atlantic Seaboard, while the previous studies encompass the Atlantic Ocean as well as North America and the British Isles. It is important to remember that the cyclogenesis exhibited within the geographical area of this study will not necessarily match that of other areas. Another significant difference is the fact that

this study was concerned exclusively with winter storms causing significant snowfall, whereas the previous studies were only concerned with storm evolution and not precipitation type or amounts. Therefore, the cyclone classifications of this present work should not be expected to exactly match classifications of previous studies.

In comparing the work of Evans et al. (1994) with this study, several similarities and differences are evident. First, the classic category of this study is similar to Evans' emerging cloud head category, especially in the jet placement. The emerging cloud head case has two meridionally separated jets, one on the northern side of the system downstream of the low and one on the cold side of the trailing cloud band upstream of the low. This is exactly the same structure as is found in the classic cases of this study; in fact, several of the classic cases had comma heads which emerged from under the baroclinic leaf as seen in infrared loops, as prescribed by this emerging cloud head category. Secondly, it would appear that the separated and warm separated classifications of this study match the instant occlusion category of Evans; however, the instant occlusion case features a distinctly separate cold-air cloud feature upstream of the frontal zone which is not initially associated with the frontal zone, whereas the comma heads of the separated and warm separated cases of this study are clearly associated with the frontal zones (in fact, some of the comma heads are initially attached to the frontal zones before separating for a period of time). The two other cyclone classifications of Evans do not appear to have any relation to this study.

While the Semple (2003) publication does not create distinct categories as Evans (1994), it does describe elements of cyclone development which are related to this study. The most notable similarity is in the comma cloud development stage. Semple proposes

two types of comma-head development following Bader (1995); type one has a continuous jet along the cold-air side of the frontal zone with warmer clouds wrapping cyclonically around the low, and type two has two distinct jets with a continuous comma head. The type two cyclone is virtually the same as the classic cases of this study, both in the cloud field and jet structure, while the type one cyclone has similarities to the warm separated cases of this study, although Semple makes no mention of a visible discontinuity between the tip of the comma head and the frontal zone as is seen in the warm separated cases of this study. Interestingly, Semple mentions that a type one comma will often develop into a type two, which is consistent with the loops of infrared imagery for the warm separated cases wherein the warmer comma head eventually merges with the frontal zone forming a continuous cloud shield as seen in the classic cases. Another similarity is Semple's mention of a separation between the cloud head and the frontal zone, as is seen in the separated cases of this study. However, Semple attributed this separation to the dry airstream of the southern jet, which, for the separated cases of this study, is too far south and west of the surface low to cause a complete comma-head separation, as shown in Fig. 5.13. Thus, Semple was most likely referring to a different feature than the type of comma-head separation within this study.

Young (1993) noted four types of cyclogenesis in looking at cyclones both over land and oceans. The cyclogenesis type which is most related to this study is what he calls "split flow cyclogenesis," wherein an upstream shortwave feature merges with a baroclinic leaf associated with a longwave trough. This cyclogenesis pattern is associated with a double jet configuration, as is the classic cyclone categorization of this present study. Young mentions specifically that this form of cyclogenesis is most

common east of the Rocky Mountains, which is exactly the area of study for this research project. Furthermore, Young's conceptual diagrams show an upper-level geopotential pattern which is nearly identical to Fig. 5.6 of this study in that it contains a negatively-tilted trough with a hint of a shortwave moving through. As with Evans (1994), Young lists a category called instant occlusion which initially seems similar to the separated and warm separated cases of this present research. However, the feature which looks like a separated comma head is in fact a preexisting feature associated with a jet or baroclinic zone; this is not the case with the separated cases of this study, wherein the separated-comma head is clearly associated with the frontal zone for the entirety of its lifespan.

One final concept of note from Young's paper is the recurring discussion of comma heads emerging from under the frontal zone with warmer cloud-tops than the frontal zone. He states that situations wherein the cloud head is well-developed and noticeably warmer than the frontal zone with a narrow cloud-free wedge in-between (a possible reference to the separated cloud-head concept) are harbingers of explosive cyclogenesis (similar to the findings of Section 6.2), implying that the separation is a part of the storm evolution. Young also states that if the cloud head becomes fragmented, it is a sign of early termination of the development cycle, which ties in with the observation that not all of the separated cases continue to develop into more mature cyclones as detailed in Section 6.2.

To summarize the connection between the cyclone categories of this study and previous research, the classic cases are very similar to well-documented cyclone evolution in the literature, the separated cases do not have much in common with previous categorizations, and the warm separated cases seem to be a part of cyclone

evolution which leads to strong cyclones. Indeed, satellite imagery and mean sea-level pressure for the warm separated cases reveals that seven of the eight cases were characterized by cyclogenesis, usually fairly strong, once the warm-separated comma head reconnected with the frontal zone. For the eight separated cases, approximately half exemplified cyclogenesis once the comma head reconnected.

### **5.3 Snow Swaths**

As detailed in Section 4.4, composites of rotated snowfall swaths were created for the three extratropical cyclone categories. Fig. 5.23 shows these snowfall composites. For each composite, the origin of the coordinate system represents the location of the surface low, while the  $x$  and  $y$  distances are the rotated coordinate space, which are dimensionless. The track of the surface low is represented as the line " $x = 0$ ", and the latitude of the "middle hour" of storm evolution (see Section 4.3) is the line " $y=0$ ". Thus, almost all of the snowfall for the cyclone cases occurred north of the low, because the composites have almost no snow where the  $y$ -coordinate is negative. In agreement with the findings of Johnston (1995), the heaviest snowfall for the separated cases occurred within a band on the southern side of the snow swath, as evidenced by the area of heavier snow from  $y$ -values of 20 to 40 and  $x$  values of 0 to 50. The classic composite also shows this feature to a certain extent, although it is not as evident. The snow swath is much more organized for the separated composite as it is nearly symmetrical in the  $x$ -direction and closely resembles the oval shape of the comma head. Also of note is the fact that the swath for the separated composite is nearly centered on the latitude of the middle hour, whereas the snow swaths of the classic and warm separated composites are centered to the east of that longitude. This suggests that snowfall within the separated

cases peaked around the middle hour, while the peak for the classic and warm separated cases occurred well beyond the middle hour.

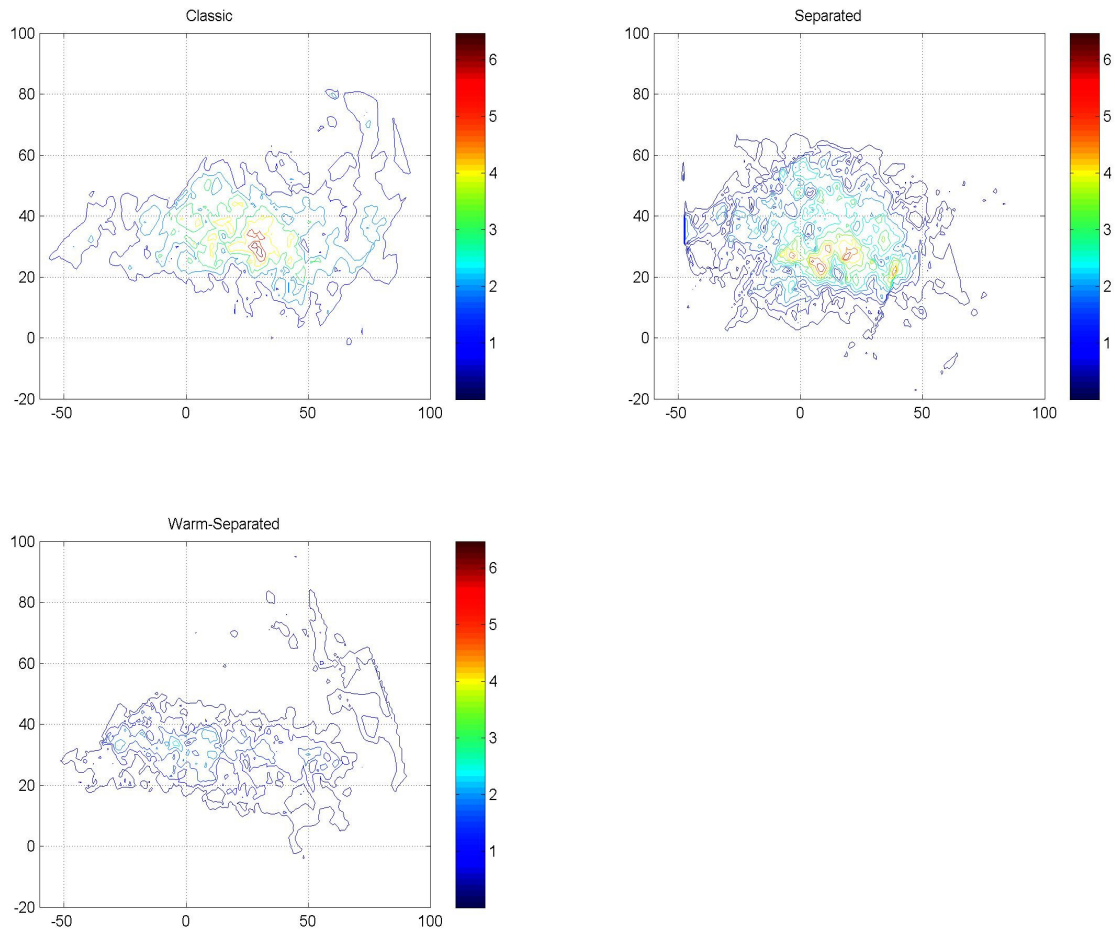


Fig. 5.23 – Composite snow swath (in) for the three cyclone categories. The swaths are rotated before compositing such that the line  $y=0$  represents the storm track and the point  $(0,0)$  is the position of the minimum MSLP point. The x and y axes are rotated coordinate systems and are thus unitless.

As with the thermodynamic variables discussed earlier in this chapter, it is useful to look at individual cases as well as composites. Figures 5.24 through 5.26 show snowfall contoured on IR satellite imagery for three cases representing the classic, separated, and warm separated cyclone categories, respectively. It is apparent that the snow swaths for these individual cases roughly match the shape of the composited swath for the

corresponding cyclone category. Fig. 5.24 shows a representative classic case. The snow swath is fairly broad to the north and west of the dry slot (narrow cloud-free area between the comma head and frontal zone). Most of the snow is confined to the southern side of the comma head, although no snow is observed southeast of the coldest cloud tops. In contrast, the representative separated case in Fig. 5.25 shows snow contours extending south of the coldest cloud tops, which is in agreement with the findings of Johnston (1995). Fig. 5.26, which represents the warm separated cases, also shows the snow swath positioned slightly south of the coldest cloud tops. In agreement with the composite, the snow swath in the classic cases extended over a longer area than the separated case, with the warm separated being in-between the two. In addition, the snow swath of the classic case is “blotchy,” meaning that the snow swath has several maxima unevenly distributed throughout which seem to be associated with the colder cloud tops. In contrast, the swath of the separated case is smoother with a more banded-like structure (a broad single band, not to be confused with multiple mesoscale bands often referred to as “banded” snowfall), while the warm separated is between the two extremes. Interestingly, the appearance of blotchy and smooth snowfall swaths for two other cases is exactly what gave rise to this present study as detailed in Section 1.

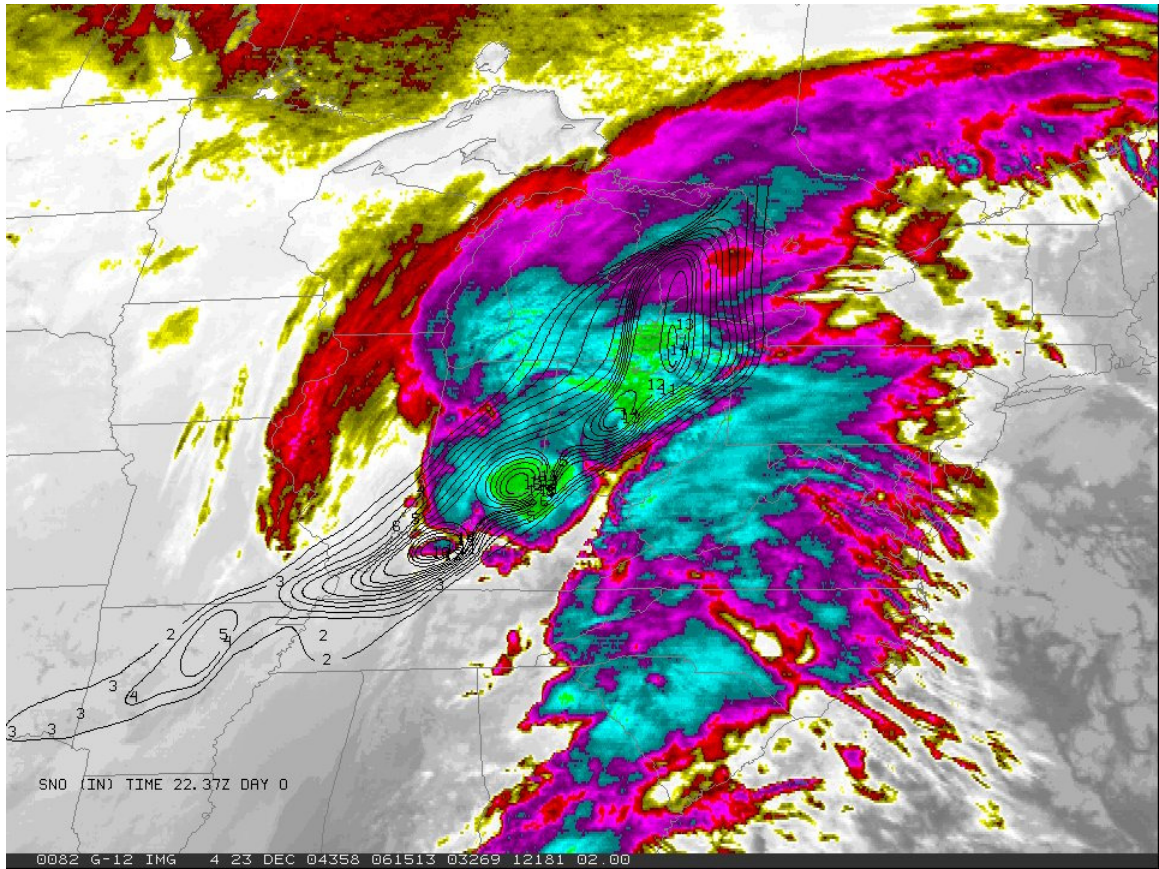


Fig. 5.24 – 10.7  $\mu\text{m}$  satellite imagery for 23 Dec. 2004 at 6:15 Z, a representative classic case, with contours of snowfall (in).

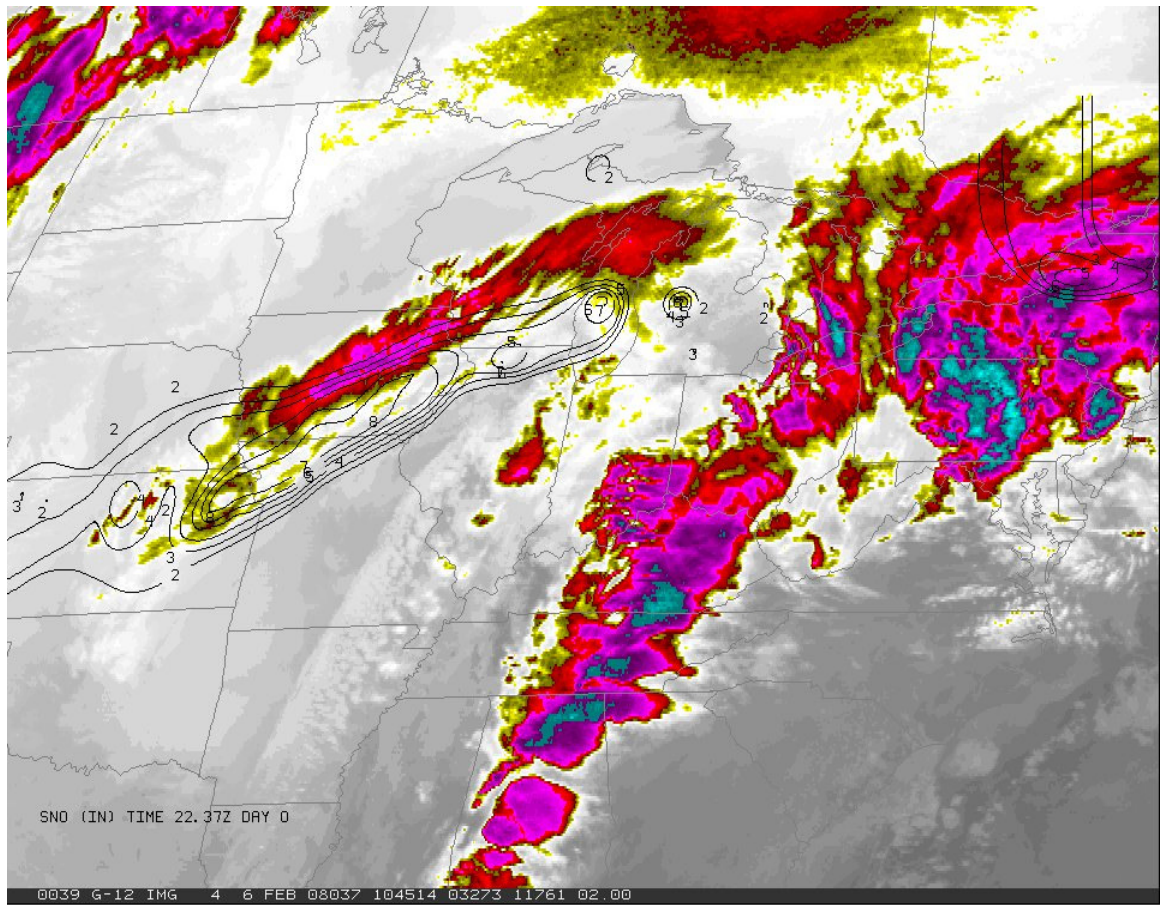


Fig. 5.25 – As in Fig. 5.24, except for 06 Feb. 2008 at 10:45 Z, a representative separated case.

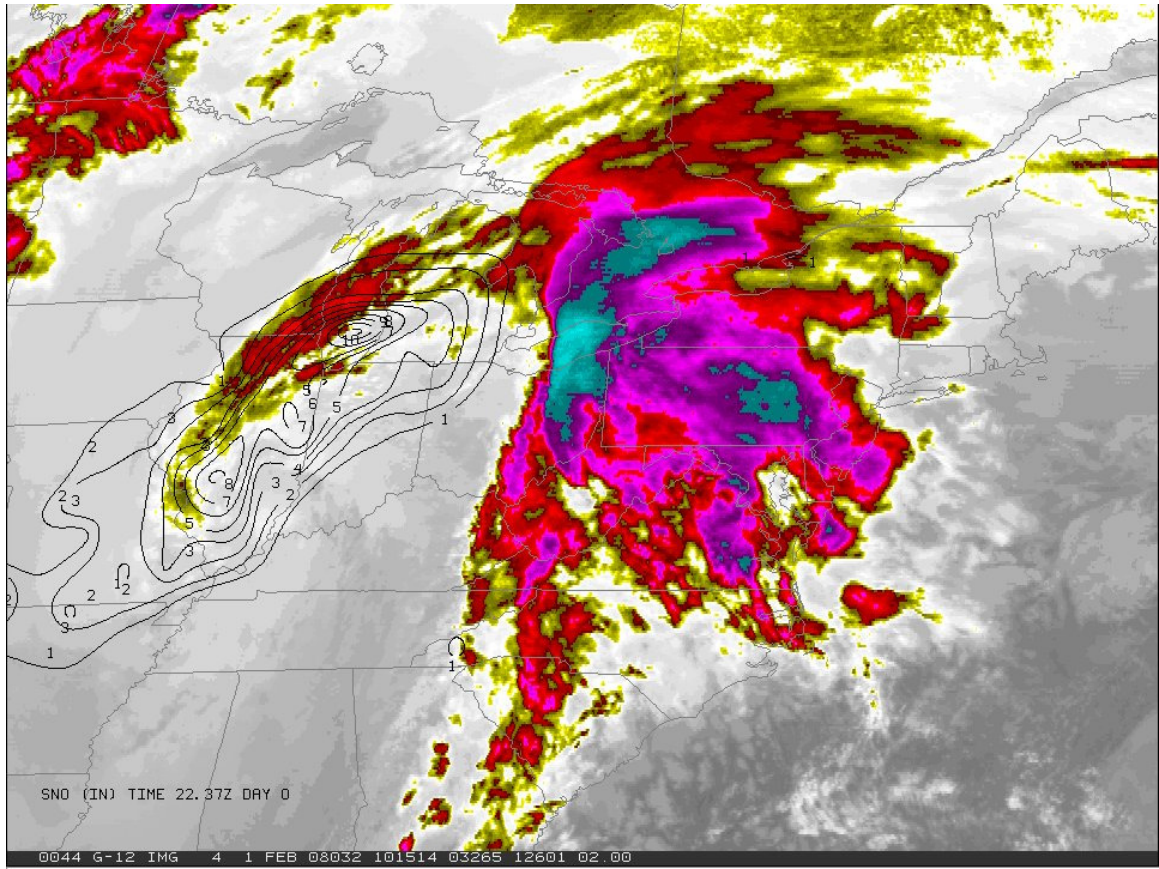


Fig. 5.26 – As in Fig. 5.24, except for 01 Feb. 2008 at 10:15 Z, a representative warm-separated case.

## 6. CONCLUSIONS

### 6.1 Causes of the Separated Comma Head

As mentioned by Semple (2003), it is difficult to divide storms into rigid classifications due to the many complicated and interconnected atmospheric variables that nature presents. This is precisely why Semple argued for a more fluid cyclone classification scheme. In this light, the objective of this study is not to find the thermodynamic causes that will completely and explicitly explain every case within the three cyclone categories. Rather, the goal is to uncover thermodynamic signatures which are found to be consistently related to the cloud structures of the cyclone categories.

The most definitive thermodynamic signature associated with the three cyclone categorizations is the position of the upper-level jet, as shown in Fig. 5.4. For the classic cases, a dual-jet configuration is present, wherein one jet resides on the northern fringes of the cyclone upstream of the low and another weaker jet wraps cyclonically around the low on the cold-air side of the frontal zone. For the separated cases, the southern jet is much further upstream and does not wrap cyclonically, while the warm separated jets are between the two extremes. The ageostrophic circulation which is associated with these jet positions aligns very well with the location of the observed clouds in infrared satellite imagery. For the classic cases, the left exit of the southern jet and the right entrance of the northern jet are aligned such that enhanced rising motion will be present between the two, as documented by Uccellini and Kocin (1987). For the separated cases and warm

separated cases, the left exit and thus the rising branch of the ageostrophic circulation of the southern jet is co-located with the colder cloud tops of the separated comma head, while the right entrance of the northern jet is positioned along the northern extent of the clouds of the frontal zone. For the warm-separated cases, the two ageostrophic circulations of the two jets are still too far apart to enhance each other, although their closer proximity places the cloud head closer to the frontal zone than the separated cases. Therefore, the lack of enhanced rising motion from the reinforcing circulations of the double-jet structure is at least partially responsible for the warmer clouds separating the comma head and frontal zone within the separated and warm separated cases.

Another persistent thermodynamic signature was the appearance or absence of a trowal, as witnessed in Fig. 5.8. As noted by Martin (1998), the trowal airstream rises (referred to as a secondary warm conveyor belt by Semple, 2003, and Young, 1993) quickly as it turns cyclonically around the surface low and is associated with clouds and precipitation northwest of the low. It is therefore reasonable that the absence of this airstream could lead to a discontinuity in the cloud and precipitation fields as is seen in the separated and warm separated cases. Indeed, the separated cases which exhibit the greatest spatial discontinuity also completely lack the trowal feature, while the warm separated cases which have a lesser discontinuity feature a weak but developing trowal. The existence of the trowal can be related to the jet position by thermal wind arguments as presented in Section 5.1. Thus, in addition to the jet dynamics mentioned earlier, the absence of the rising motion of the trowal airstream is probably also related to the observed lack of continuous cold clouds within the separated and warm-separated cases.

## 6.2 Forecasting Implications

From an operational weather forecasting perspective, this research is useful in two ways: knowledge of cyclone classifications can give insights into future storm evolution, and links between cyclone categories and resulting snow swaths can assist forecasters in snowfall nowcasting.

Analysis of the infrared satellite imagery loops for the eight cases of the three categories shows consistent trends that are intrinsic to each group. The evolution of the classic cases in this study aligns very well with the classifications of previous work detailed in Section 2.1. For the separated cases, the separated comma head reconnected with the frontal zone as seen in infrared imagery for six of the eight cases. For the cases in which the separated comma head reconnected, the average duration of separation was eight hours. Four of the cases featured cyclogenesis as the features merged, and the remaining four either showed steady MSLP or cyclolysis. More significantly, the separated comma heads for seven of the eight of the warm-separated cases eventually merged with the frontal zone, and six of the eight exhibited a pressure fall within the surface low after the merger (as mentioned in Section 5.2, the warm separated cases appear to be a part of cyclone evolution which leads to strong storms). Two of those cases exhibited a substantial surface pressure decrease of at least 15 mb in 24 hours or less. These MSLP changes are summarized in Tables 6.1 and 6.2. Averaging the pressure falls for all the warm-separated cases showed an average decrease of 8 mb in 15 hours, a notable deepening of the low. Therefore, if a forecaster discovers a storm exhibiting the likeness of a warm separated cyclone, it can be assumed that the cyclone

will likely deepen with the next 15 hours, which can then be supported by forecast model data.

Table 6.1 – MSLP changes for the separated cases.

Case	Separated comma head rejoined?	If rejoined, pressure drop in time interval
06-Feb-08	Yes	5 hPa / 12 hrs
11-Mar-00	Yes	4 hPa / 15 hrs
13-Mar-99	No	n/a
13-Mar-06	Yes	Pressure rise
16-Dec-07	Yes	4 hPa / 6 hrs
18-Feb-00	Yes	Pressure rise
24-Dec-02	Yes	5 hPa / 6 hrs
26-Nov-01	No	n/a

Table 6.2 – MSLP changes for the warm-separated cases.

Case	Separated comma head rejoined?	If rejoined, pressure drop in time interval
01-Dec-96	Yes	15 hPa / 24 hrs
01-Dec-04	Yes	19 hPa / 15 hrs
01-Feb-08	Yes	No drop
04-Mar-08	Yes	6 hPa / 12 hrs
09-Feb-01	No	n/a
09-Nov-00	Yes	4 hPa / 12 hrs
10-Jan-06	Yes	6 hPa / 12 hrs
27-Feb-97	Yes	8 hPa / 12 hrs

The other forecasting implication of this study is snowfall nowcasting. As mentioned in Section 1, this research originated from noting the apparent connections between different snowfall swaths and infrared satellite imagery. It was noted that one case produced a “blotchy” snow swath (the swath had several maxima unevenly distributed throughout), while another produced a more organized swath consisting of a single narrow band. As it turned out, this dichotomy of snowfall swath properties is characteristic of the three cyclone categories of this study. Specifically, the classic cases exhibited a blotchy snow swath, while the warm separated cases were more organized,

and finally the swaths of the separated cases were usually organized into a single narrow band on the southern edge of the comma cloud. This could be useful to operational nowcasting in two ways. First, the appearance of a classic cyclone implies that there will be a greater range of snowfall values within the cloud shield of the comma head (the blotchy characteristic), while the observation of a warm separated or separated cyclone implies a more even distribution throughout an organized snow band. Secondly, if the cyclone is a warm separated case or particularly if it is a separated case, the heaviest snow would be expected just to the south of the coldest cloud tops of the comma head; conversely, if it is a classic case, the snowfall would be concentrated towards the southern side of the comma head, although not extending southward of the coldest clouds.

### **6.3 Future Work**

It would be useful to know the snowfall rate at the various stages of storm evolution for each case, which would help in understanding precisely which part of the snowfall swaths were associated with which parts of the clouds. Devising a metric for total snowfall for a storm such as the average snow depth multiplied by the area of the snow swath might yield interesting data of the snow producing capabilities of the different cyclone classifications.

One avenue of assessing storm dynamics which was not pursued in this study is tracking air parcel trajectories. As theorized in Section 6.1, the absence of a trowal airstream was stated to be partially responsible for the lack of continuous cold clouds for the separated cases. Tracking individual parcels along isentropic trajectories yields valuable information on the three-dimensional airstreams within a storm, and so the

application of this technique to the cases of this study could more thoroughly validate the presence or absence of a trowal within each case and the role it plays in clouds and precipitation.

The period of study for this research was limited by the period of archived satellite imagery. Future research could make use of other archives, and in so doing extend the period of study to include more cases. More cases for each category would allow for the elimination of “marginal” cases (that is, cases which barely meet the cloud top temperature and spatial requirements) as well as providing more cases in general, yielding more statistically rigorous results.

## REFERENCES

- Bader, M. J., G. S. Forbes, J. R. Grant, R. B. E. Lilley, and A. J. Waters, 1995: *Images in Weather Forecasting: A Practical Guide for Interpreting Satellite and Radar Imagery*. Cambridge University Press, 499 pp.
- Beckman, S. K., 1987: Use of enhanced IR/visible satellite imagery to determine heavy snowfall areas. *Mon. Wea. Rev.*, **115**, 2060–2087.
- Beebe, R. G., and F. C. Bates, 1955: A mechanism for assisting in the release of convective instability. *Mon. Wea. Rev.*, **83**, 1–10.
- Carlson, T. N., 1980: Airflow through midlatitude cyclones and the comma cloud pattern. *Mon. Wea. Rev.*, **108**, 1498–1509.
- Clark, J. D., 1983: *The GOES User's Guide*. U.S. Department of Commerce, 164 pp.
- Dixon, R. S., Browning, K. A., and Shutts, G. J. 2002: The relation of moist symmetric instability and upper-level potential-vorticity anomalies to the observed evolution of cloud heads. *Quart. J. R. Meteorol. Soc.* **128**, 839–860.
- Evans, M. S., D. Keyser, L. F. Bosart, and G. Lackmann, 1994: A satellite-derived classification scheme for rapid maritime cyclogenesis. *Mon. Wea. Rev.*, **122**, 1382–1416.
- Grim, J. A., R. M. Rauber, M. K. Ramamurthy, B. F. Jewett, and M. Han, 2007: High-resolution observations of the trowal–warm-frontal region of two continental winter cyclones. *Mon. Wea. Rev.*, **135**, 1629–1646.
- Hakim, G. J., and L. W. Uccellini, 1992: Diagnosing coupled jetstreak circulations for a northern plains snowband from the operational Nested Grid Model. *Wea. Forecasting*, **7**, 26–48.
- Han, M., R. M. Rauber, M. K. Ramamurthy, B. F. Jewett, and J. A. Grim, 2007: Mesoscale dynamics of the trowal and warm-frontal regions of two continental winter cyclones. *Mon. Wea. Rev.*, **135**, 1647–1670.
- Harrold, T. W., 1973: Mechanisms influencing distribution of precipitation within baroclinic disturbances. *Quart. J. Roy. Meteor. Soc.*, **99**, 232–251.

- Holton, J. R., 2004: *An Introduction to Dynamic Meteorology*. 4th ed. Academic Press, 511 pp.
- Johnston, E.C., 1995: Updated satellite technique to forecast heavy snow. *Wea. Forecasting*, **10**, 1995, 219-228.
- Martin, J. E., 1998: The structure and evolution of a continental winter cyclone. Part I: Frontal structure and the occlusion process. *Mon. Wea. Rev.*, **126**, 303–328.
- \_\_\_\_\_, 1998: The structure and evolution of a continental winter cyclone. Part II: Frontal forcing of an extreme snow event. *Mon. Wea. Rev.*, **126**, 329–348.
- \_\_\_\_\_, 1999: Quasi-geostrophic forcing for ascent in the occluded sector of cyclones and the trowal airstream. *Mon. Wea. Rev.*, **127**, 66–84.
- Menzel, W. P., and J. F. W. Purdom, 1994: Introducing GOES-I: The first of a new generation of Geostationary Operational Environmental Satellites. *Bull. Amer. Meteor. Soc.*, **75**, 757–781.
- Mesinger, F., and Coauthors, 2006: North American regional reanalysis. *Bull. Amer. Meteor. Soc.*, **87**, 343–360.
- Moore, J. T., C. E. Graves, S. Ng, and J. L. Smith, 2005: A process oriented methodology toward understanding the organization of an extensive mesoscale snowband: A diagnostic case study of 4–5 December 1999. *Wea. Forecasting*, **20**, 35–50.
- NCDC, 2006: Surface land daily cooperative summary of the day. DSI-3200, 19 pp. [Available from National Climatic Data Center, 151 Patton Ave., Asheville, NC 28801; also available online at <http://www1.ncdc.noaa.gov/pub/data/documentlibrary/tddoc/td3200.pdf>.]
- Novak, D. R., L. F. Bosart, D. Keyser, and J. S. Waldstreicher, 2004: An observational study of cold season–banded precipitation in northeast U.S. cyclones. *Wea. Forecasting*, **19**, 993–1010.
- Pauley, P. M., and S. J. Nieman, 1992: A comparison of Quasigeostrophic and nonquasigeostrophic vertical motions for a model-simulated rapidly intensifying marine extratropical cyclone. *Mon. Wea. Rev.*, **120**, 1108–1134.
- Rutledge, G.K., J. Alpert, and W. Ebuisaki, 2006: NOMADS: A climate and weather model archive at the National Oceanic and Atmospheric Administration. *Bull. Amer. Meteor. Soc.*, **87**, 327-341.
- Schultz, D. M., and P. N. Schumacher, 1999: The use and misuse of conditional symmetric instability. *Mon. Wea. Rev.*, **127**, 2709–2732.

- \_\_\_\_\_, D. M., 2001: Reexamining the cold conveyor belt. *Mon. Wea. Rev.*, **129**, 2205–2225.
- Semple, A.T., 2003: A review and unification of conceptual models of cyclogenesis. *Meteorological Applications*, **10**, pp 39-59.
- Uccellini, L.W., and Kocin, P.J., 1987: The interaction of jet streak circulations during heavy snow events along the east coast of the United States. *Wea. Forecasting*, **2**, 289-308.
- Wallace, J. M., and P. V. Hobbs, *Atmospheric Science, An Introductory Survey*, 467 pp., Academic, San Diego, Calif., 1977.
- Weldon, R. B., 1986: Synoptic scale cloud systems. In P.S Parke (ed.), *Satellite Imagery Interpretation for Forecasters*, Temple Hills, Md., National Weather Association, Meteorological Monographs 2–86, 1, pp. 2.A.1–35.
- Young, M. V., 1993: Cyclogenesis: Interpretation of satellite and radar images for the forecaster. Forecasting Research Division Tech. Rep. 73. [Available from Forecasting Research Division, Meteorological Office, London Rd., Bracknell, Berkshire RG12 2SZ, United Kingdom.]
- Zishka, K. M., and P. J. Smith, 1980: The climatology of cyclones and anticyclones over North American and surrounding ocean environs for January and July, 1950–77. *Mon. Wea. Rev.*, **108**, 387–401.

## **Appendix 1. Forecaster Checklist**

This section describes how a forecaster might apply the results of this study to forecasting snowfall from the comma head of an extratropical cyclone. One important consideration is the forecast lead-time potential of the various topics discussed within this research. The following discussion details two different lead-time scenarios wherein this research could be of help to forecasters. This is followed by a checklist which reproduces the same information as it might be used in an operational forecasting environment.

Firstly, the jet concepts discussed earlier can be used in analyzing model forecasts for lead times of 12-36 hours, or whenever the forecaster is confident in reliability of the model-forecasted upper-level winds. Plotting the jet positions in the vicinity of the surface low pressure could reveal whether the storm will take on the characteristics of the classic or separated cases of this study. As detailed in Section 5.1, if two jets are present in the vicinity of the cyclone, the position of those jets relative to one another has important implications on the type of storm which develops. From that point, the forecaster can know whether to expect a continuous or separated comma head, and can thus make broad conclusions about the resulting snow swath as detailed in Section 5.3

At forecast lead times of 3-12 hours, the cyclone should already be developing and its structure should be appearing on satellite imagery. At this point, the forecaster should already be expecting the cyclone to take the form of a classic or separated storm (based on the information provided in the previous paragraph), and the satellite imagery can

know be used to verify this prediction. If a separated cyclone is expected, a disconnect between the clouds of the developing comma head and frontal zone should develop. If a classic cyclone is expected, a comma head should be developing west of the frontal zone or emerging from under the clouds of the baroclinic zone. Once it can be verified that a particular cyclone category is occurring, the forecaster can begin to adjust the certainty in his or her snowfall forecast for the appropriate regions relative to the various areas of the comma head. Specifically, if a separated case is occurring, the forecaster can increase confidence in probability of snowfall along and to the south of the comma head, whereas for a classic case, the probability should be highest in the area directly under the comma head.

Hours before an event of concern (e.g. traffic commute, school closure deadline, etc.):

- 12-36: use NWP (numerical weather prediction) models to determine whether a dual-jet configuration will occur with the developing storm, and whether those two jets will lead to a classic or separated cyclone
- 6-12: satellite imagery should begin to confirm the predicted cyclone type, pops (probability of precipitation forecasts) should be adjusted to reflect this
- 3-6: satellite should be able to completely verify the forecasted cyclone type, radar should indicate whether precipitation is developing in expected area
- 0-3: surface observations should begin to reflect expected snow swath characteristics, forecast-based decisions such as school closures can be enacted

## Appendix 2. Inconclusive Diagnostics

This section details several diagnostics used throughout the course of this research which had inconclusive results. This does not mean that these features did not have a roll in the cyclones of this study; rather, it means that conclusive results were not attainable with the methods attempted. Future work might yield better results with these diagnostics.

Many authors have used the concept of CSI (conditional symmetric instability) to diagnose areas of storms with potential for banded snowfall (Martin, 1998b, Moore et al., 2005). However, there are numerous complications involved in finding areas which will realize the potential instability from CSI, including the necessary conditions of moisture and a lifting mechanism (Schultz and Schumacher, 1999). One common means of diagnosing the presence of CSI is plotting cross sections and plan views of EPV (equivalent potential vorticity). As discovered in this study, however, there are numerous complications even in that computation, such as whether to use the somewhat-noisy geostrophic wind or total wind, and whether to use  $\theta_{es}$  (saturated equivalent potential temperature) or  $\theta_e$ . All these variants were taken into consideration and plotted for the cyclone categories of this present study, and yet no clear connections between CSI and areas of snowfall were discovered. There were areas of negative EPV and saturation within the storms (a condition usually diagnosed as containing CSI), but most of these were in the upper areas of the storm (e.g. 500-300 mb) which probably were not

responsible for the majority of precipitation observed at the surface. In the end, all of the uncertainty involved in the CSI calculations and determinations prevented its inclusion in this present study.

Another common thermodynamic diagnostic which is absent from this study is frontogenesis. As with CSI, many authors have attempted to use frontogenesis to explain areas of heavy or banded snowfall (Martin 1998b, Moore et al. 2005, Han et al. 2007). It was attempted within this research to follow the lead of previous publications in using the Petterssen frontogenesis equation to find areas within the storms of frontogenesis potential. As was the case with CSI, the resulting plots were too inconclusive to create any meaningful results.

Three extratropical cyclone airstreams (also known as conveyor belts) have been noted extensively in the literature: the WCB, CCB, and dry airstream (Han et al., 2007). The first two were discussed frequently in this study (see Section 2.1), but the dry airstream was not discussed. This exclusion of the dry airstream was a result of difficulty in verifying its existence in the NARR relative humidity fields for this study. It is important to note that errors in the moisture fields of the NARR could have been the cause of this, and thus the dry airstream could still have influenced the development cyclones of this study; it simply was not possible to verify this link with the data and methods available.